TO DEVELOP AND EVALUATE PICKERING NANOEMULSION CONTAINING BIOACTIVE COMPOUNDS FROM PASSION FRUIT PEEL AND STABILIZED WITH STARCH NANOPARTICLES

CHAPTER 4

CHAPTER 4

DEVELOPMENT AND EVALUATION OF PICKERING NANOEMULSION CONTAINING BIOACTIVE COMPOUNDS DERIVED FROM PASSION FRUIT PEEL AND STABILIZED WITH STARCH NANOPARTICLES

4.1. Introduction

Passion fruit *(Passiflora edulis)* is a nutritious fruit that is presently being used for profit by the pharmaceutical, cosmetic, and food production industries [1,12]. Although, the peel of this fruit is enriched with biologically active compounds specially carotenoids, anthocyanins, phenolic groups, etc., more than 50 % of the whole fruit is discarded as waste, which is composed of peel and seeds [50]. As stated in **Chapter 3,** the extraction process followed was able to extract 91.4 % of total carotenoids and other bioactive compounds present in passion fruit peel (PFP) using olive oil (OO) as the solvent and produced carotenoids-enriched olive oil (CEOO) of good quality. However, Ruiz-Montañez et al. [54] mentioned about the significant degradation of oil-extracted carotenoids. Carotenoids are sensitive to light, oxygen and/or heat and are lipophilic in nature with low solubility in aqueous solution and poor bioavailability in crystalline form, which restrict their direct use in aqueous food products [25,43].

Emulsion is a promising strategy for incorporating lipophilic bioactive substances in a carrier system to maintain their bioactivity while solubilizing in an aqueous food system [9,15,20]. Emulsions are thermodynamically unstable due to four processes, namely, coalescence, creaming, flocculation, and Ostwald ripening [46]. Research related to production of stable food grade emulsion is still going on. Pickering emulsion can be used to stabilize the emulsions due to the strong anchoring energy and specific surface interaction (reduced interfacial tension) [9,14,34]. Pickering emulsion hampers or possibly completely blocks the Ostwald ripening [34]. Polysaccharides derived particles are most suitable as emulsifiers due to their availability, biodegradability and biocompatibility [9]. Li et al. [34] produced a Pickering nanoemulsion using 0.2 % starch as an emulsifier that showed no coalescence and size variation for up to 2 months.

Due to their size and hydrophilic nature, natural starch particles are ineffective as emulsifiers, therefore, some modification is necessary to increase the starch's emulsifying abilities [29,34]. Mostly chemical, physical, and enzymatic methods are used to enhance the functionality of starch by reducing the size (nano scale size) and increasing its

solubility. However, due to their great propensity to agglomerate, particularly when the particles are in the form of dry powders, starch nanoparticles (StNPs) produced by the conventional chemical processes have limited practical use, besides giving low yield and generating chemical waste that causes serious environmental effects [29]. Similarly, enzymatic treatment is associated with high cost, serious recovery problem, and specificity of enzyme activity.

Physical modifications of starch give approximately 100 % yield in less time [2]. Ultrasound (US) and high-pressure homogenization (HPH) are two physical alteration procedures that have been applied as substitute other methods to create nanoemulsions. In HPH, suspension is passed through a small nozzle that causes mechanical stress, cavitation and turbulence of the medium because of which nanoparticles are formed [26,39,59]. In US treatment, due to the collapse of cavitation bubbles, high pressure and temperature are generated that favour formation of nanoparticles [4]. However, longer US and HPH treatments can re-agglomerate the nanoparticles again [42,59].

Several researchers have used US to produced nanoparticles [4,29] in acid or alcohol medium, but to the best of our knowledge no study has been reported on using water as the medium for the synthesis of starch nanoparticles by US that can directly be used in nanoemulsion development without any separation process. Similarly, several researchers have used HPH for nanostarch production [7,59] and have reported that prior to HPH treatment, some additional steps have to be performed for efficient production. Liu et al. [37] reduced the particle size of starch from 3–6 μm to 10–20 nm using pressure of 207 MPa, which is too high for industrial use, as in industries mostly 200-500 bar pressure is used [59]. Calligaris et al. [7] mentioned that US treatment followed by HPH treatment gave significantly lower particle size than samples processed in the reverse order. Production of new functional starches with biological activity is always of interest for industries as well as researchers. Xinde et al. [61] was able to produce high carotenoids enriched starch powder by encapsulating it.

Thermal degradation and mechanical performance of native starch limit its application in food industries. Thermal analysis is a set of techniques for the quick evaluation of thermal stability, adsorbed water amount, crystal water amount, thermal degradation kinetics, and decomposition parameters [53]. Differential scanning calorimetry (DSC) and Thermogravimetric analysis (TGA) are the prevalent techniques followed to study the thermal behaviour of polymers [40,53]. Thermal properties of StNPs, mainly the degradation and stability processes are important criteria used in starch

nanoparticles-based food industry such as extrusion cooking at high temperature [6], fat replacers, and emulsion stabilizers [55] to process at different high temperature, and during processing to judge their suitability [6]. So, knowledge of thermal degradation and monitoring the kinetics of StNPs are essential to understand their behaviour during thermal processing [44]. In recent years, several researchers have studied the thermal behaviour and decomposition kinetics of starch from rice, wheat, corn, and potato [49], sugarcane straw [53], sweet potato starch [40], natural extract of chitosan-starch [41], and ultrasonicated purple taro starch [44].

So far, no study has been reported on the production of carotenoids-enriched starch-based nanoemulsion and carotenoids-enriched starch nanoparticle powder using naturally available carotenoids and no study has been found on the thermal degradation kinetics of physically modified (HPH and US) corn StNPs. The aim of the work reported in this chapter was to produce stable nanoemulsion of carotenoids present in passion fruit peels using thermally stable starch nanoparticles developed by a combination of US and HPH treatments of corn starch dispersed in aqueous medium using a pressure range suitable for industrial use and study their properties. The obtained carotenoids-enriched starch nanoparticles were characterized. The novelty of this work was to develop a simple, chemical free and environment-friendly approach for the preparation of thermally stable starch-based bioactive-enriched starch nanoparticles as well as stable nanoemulsion using fruit waste as source material for the bioactives.

4.2. Materials and Methods

4.2.1. Materials

Normal starch (corn) was obtained from Sona Fruits Traders (Uttar Pradesh, India) and olive oil from Aar Gee Formulations (Himachal Pradesh, India). Passion fruit (*Passiflora edulis*) was procured from a farmer in Bishnupur District, Manipur, India. HPLC grade chemicals were procured from Sigma-Aldrich. The chemicals utilised in this study were of analytical grade. All experiments were performed in triplicates (except for instrumental analysis).

4.2.2. Sample preparation

4.2.2.1. Preparation of ultrasonic-treated (US) starch nanoparticles

Native corn starch (NS) powder (1, 3, and 5 g) was suspended in 100 mL of milli-Q-water in a breaker that was placed in a thermostatically controlled and jacketed glass unit maintained at 10 ± 3 ℃. The suspension was sonicated in a probe sonicator (U500,

Takashi, Japan) with power set to 90% amplitude and the pulse mode set to on/off for 3s/3s during a time range of 15 -150 min. Aliquot was sampled at regular intervals and the particle size and polydispersity index (PDI) were directly measured [4] and optimized time was calculated taking into consideration the lowest PDI and size. The treated starch was coded US-StNP.

4.2.2.2. High pressure homogenization (HPH) of US-StNP

The optimized US treated starch (US-StNP**)** suspension was homogenized directly using a laboratory scale high-pressure homogenizer (GEA, Lab homogenizer, Italy) at optimized pressure condition of nanoemulsion preparation (described below). The homogenised starch suspension was lyophilized. The freeze dried optimized high pressure homogenized starch suspension was coded as HP-US-StNP.

4.2.2.3. Preparation of carotenoids enriched StNPs-based nanoemulsion

The process for obtaining CEOO oil is described in **Chapter 3**. Coarse emulsion was prepared by mixing the CEOO (1-10%) with US-StNP (optimized treatment time based on particle size and PDI) using a T25 Ultra-Turrax (IKA Works, USA) high-speed mixer for 5 min at 12500 rpm. The starch range taken for nanoemuslion formation was 1-5 %. Other independent parameters selected in this study were concentration of carotenoids enriched oil (1-10%) and homogenizing pressure (100-500 bar). The experimental design is given in **Table 4.2.** Initially, the number of passes used was 1, 3, 5, 7, and 10 and eventually 5 numbers of passes was selected based on particle size analysis, temperature of the emulsion, and separation of the emulsion.

The well mixed coarse emulsion was thereafter homogenized in a two-stage high-pressure homogenizer (GEA, Lab homogenizer Panda Plus 2000, Italy) as per the experimental design **(Table 4.2)**. Thereafter, 500 mL of coarse emulsion were processed for each experimental set, and pressure of the second stage was adjusted to about 1/10 of that of the first stage [59], which is an industrial practice followed to achieve better homogenization. The freeze dried nanoemulsion powder was coded as C-HP-US-StNP and the developed optimized starch-based emulsion was coded as C-HP-US-StNE.

4.2.2.4. Preparation of carotenoids enriched StNPs

To obtain the carotenoids enriched starch nanoparticles powder, 5 % of carotenoids enriched oil was added to 5% US-StNP and the nanoemulsion was prepared as described

above. The nanoemulsion was freeze-dried (LYOLAB, Lyophilization systems, India). This powder was coded as C-HP-US-StNP.

4.2.3. Particle size and polydispersity index of StNPs

The average particle size of the prepared suspensions of NS, US-StNP, HP-US-StNP and C-HP-US-StNP was measured through dynamic light scattering (DLS) using a Zeta potential and Nano particle size analyser (Nanoplus-3). The average size (Z, nm) and polydispersity index (PDI) were measured to characterize the size of the particles and their size distribution pattern. Mean values of five readings are reported.

4.2.4. Colour of StNPs

Colour of NS, US-StNP, HP-US-StNP and C-HP-US-StNP was measured using Hunter CIELAB colour meter.

4.2.5. Flow properties of StNPs

The repose angle and Hausner ratio (HR) were measured to understand the flow properties of StNPs. Hausner ratio was calculated by using **Eq. 4.1** [61].

$$\mathrm{HR} = \frac{\rho_{\mathrm{tapped}}}{\rho_{\mathrm{aerated}}} \tag{4.1}$$

where ρ_{aerated} and ρ_{tapped} was the bulk density of sample powder observed under aerated and tapped conditions, respectively. HR value of powders separates the cohesive, difficult-to-fluidize group of powder from the free-flowing, easily fluidized group, in terms of the powder flowability. Classification of flowability based on HR is reported in **Table 4.1**.

Table 4.1. Flowability classification of powders based on several indices [61].

Flow characteristic	Flow index	HR	α
Non flowing	<1	>1.4	>60
Cohesive	2-4	>1.4	>60
Fairly free flow	4-10	1.25-1.4	45-60
Free-flowing	>10	1-1.25	30-45
Excellent flowing	>10	1-1.25	10-30
Aerated	>10	1-1.25	<10

The static repose angle was measured according to the conventional method given by Xinde et al. [61]. Briefly, the filter, shaking chute, and funnel were used for dropping

the StNPs onto a sheet of paper with graded concentric circles that is axial with the funnel opening.

The repose angle **(**α) was expressed as **Eq. 4.2.**

$$\alpha = \tan^{-1}\left(\frac{2H_p}{D_p - d_f}\right) \quad (4.2)$$

where 'D_p' and 'd_f' was the base diameter of powder samples (cone) and the outlet portion of funnel, respectively, and 'H_p' was cone height of the powder samples. With the above method, determining the repose angle for cohesive and free-flowing powders was simple and accurate. The classification of flowability is reported in **Table 4.1**.

4.2.6. Swelling power and solubility of StNPs

Swelling power and solubility were calculated by using the same method as adopted by Kaur and Gill [28]. In a nutshell, 1 g of NS and StNPs was suspended in milli-Q water, and the aqueous suspension was heated at 95 ℃ for 1 h while being constantly stirred at 120 rpm. The suspension was then centrifuged for 10 min at 3000×g while it was cooled to 30 ℃ for 30 min and swelling power was determined as sample weight per gram of sample. By transferring the suspension to Petri plates, drying it at 110 ℃ for 12 h in hot air oven, cooling it to room temperature in a desiccator, and weighing the dry particles, the solubility of the mixture was calculated.

4.2.7. Fourier transform-infrared spectroscopy (FTIR) of StNPs

Using an FTIR spectrophotometer (IMPACT 410, USA), the infrared spectra of NS and StNP samples were captured in accordance with Choi et al. [9]. Briefly, KBr was added to the samples and mixed properly, shaped into pellets, and then analysed using attenuated total reflectance spectroscopy in the 4000-400 cm^{-1} wave range. By noting the height of the absorbance bands from the baseline in the spectra, intensity measurements were made.

4.2.8. X-ray diffraction (XRD) of StNPs

XRD was performed to analyse the crystalline structure of NS and StNPs using powder X-ray diffractometer (D8 FOCUS, Bruker Axs, Germany) having CuKα source functioning at 30 kV and 15 mA. Data were obtained at 25 ℃ and the 2θ scan was done between 5 º to 35 º with a scanning rate of 0.25 °/min and sampling interval of 0.02 ° [9]. The MS Excel data was converted to the graph-making programme using Origin software (Origin Pro 8E, Origin Lab, USA).

4.2.9. Morphology of of StNPs

Surface morphology of the NS and StNPs was analysed using a scanning electron microscope (SEM) (JSM 6390LV, JEOL, Japan). Dried sample powders were placed on double-sided adhesive conductive carbon tape attached to a stub and coated with platinum, under vacuum. 20 kV voltage was set during the experiments. For observation, working distances of 150X and 500X were used [2].

4.2.10. Rheological properties of StNPs

Briefly, 1 % and 5 % (w/v) NS and StNP samples were prepared for the rheological test and tests were performed using the method developed by Herrera et al. [48] with slight modification. Briefly, dried samples were dispersed in milli-Q water using T25 Ultra-Turrax (IKA Works, Inc., NC, USA) homogenizer at 15,000 rpm for 30 min . The rheological tests were performed using a rheometer (Anton Paar, Austria) with a cone and plate (30 mm diameter, 53 μm gap). Each sample was equilibrated at 25 ℃ for 2 min prior to each test. Relationship between the apparent viscosity and shear rate of the StNPs suspensions were performed through the continuous shear test. The shear rate range was between 0.01 and 100 s^{-1}.

4.2.11. Differential scanning calorimetry (DSC) of StNPs

DSC analysis was performed to observe the energy associated with heating or cooling process in a closed system and measure the change in the physical properties of the sample with change in temperature against time. According to Kim et al. [29], a differential scanning calorimeter (DSC, Netzsch, Germany) was used to study the thermal transition parameters of NS and all StNPs in a closed system. Briefly, in an aluminum DSC pan, approximately 9 mg (total weight) sample solution containing StNPs to water ratio of 1:2 was placed and hermetically sealed. Before analysis, the sealed pan with sample was equilibrated at 4 ℃ for 2 h and during the equilibraton time, pan was shaken at half an hour interval. After that, sample DSC pan was heated at a rate of 5 ℃/min, scanning from 25 °C to 120 °C. An empty pan served as the reference for the DSC instrument's calibration with indium prior to the analysis.

4.2.12. Thermogravimetric analysis (TGA) of StNPs

Thermal stability of NS and StNPs samples was determined using a Thermo gravimetric analyser (TGA, Netzsch, Germany) with inert nitrogen gas with flow rate of 20 mL min^{-1}, temperature ranging between 30 ℃ and 600 ℃, and a temperature rise rate

of 10 °K/min [2]. Lid free crucible made of alumina was used as sample holder. Same amount of starch was used and the change in mass of thermally treated starch was recorded.

4.2.13. The total carotenoids (TCC) and β-carotene content of nanoemulsion

TCC and β-carotene content of optimized StNP based nanoemulsion prepared with CEOO and untreated olive oil (UOO) were analysed for carotenoids content using the same method developed by Caravalho et al. [8] with small alterations. Shortly after adding 15 mL sample to 25 mL of acetone, the mixture was put into a sintered funnel and filtered under vacuum. This process was continued three times or till sample lost its colour. The extracted substance was put into a separatory funnel (500 mL) with 40 mL of petroleum ether and butylated hydroxy toluene (0.1%) as the extraction medium mixture. To avoid emulsion formation, the acetone was eliminated by gradually introducing ultrapure water (Milli-Q - Millipore). The aqueous phase was thrown away. Up till no residual solvent remained, this process was done for four times. The extract was then funnelled into a 50 mL volumetric flask that contained 15 g of anhydrous sodium sulphate. The volume was filled up with petroleum ether, and absorbance was read at 450 nm. TCC was calculated using the following formula (**Eq. 4.3**)

$$\text{TCC (µg/100 mL)} = \frac{A \times v \times 10^4}{E^{1\%}_{1\,cm} \times V} \times 100 \quad (4.3)$$

where A is the absorbance, V and v is the total volume of extract (mL) and total volume of juice (mL) and $E^{1\%}_{1\,cm}$ is the extinction coefficient (2592) for β-carotene in hexane.

β-carotene was evaluated using the same method developed by Hsu et al. [23], the details of the method is mentioned in **Chapter 6.**

4.2.14. Total phenolic content of nanoemulsion

Folin–Ciocalteu Reagent colorimetric method was adopted for determination of total phenolic content of nanoemulsion [16] and detailed procedure is mentioned in **Chapter 3**.

4.2.15. Antioxidant activity (2,2-diphenyl-1-picrylhydrazyl) (DPPH) free radical scavenging activity of nanoemulsion

DPPH antioxidant activity determines the hydrogen donating capacity of molecules and does not produce oxidative chain reactions or react with free radical intermediates.

Antioxidant activity (DPPH activity) of sample was evaluated by using the method adopted by Chutia et al. [10] and given in detail in **Chapter 3.**

4.2.16. Heat and freeze-thaw stability of nanoemulsion

Thermal stability (heat and freeze-thaw) of developed nanoemulsions was measured by the method developed by Choi et al. [9] with slight modifications. Briefly, fresh emulsion (prepared using the optimized conditions) was heated for 10 min at 100 ℃ before being let to cool to room temperature naturally. Freshly made emulsions were frozen (-18 ℃) for 24 h, then stored at ambient temperature until the emulsion's temperature approached the ambient level in order to test for freeze-thaw stability. Using a digital camera, changes in emulsion morphology were documented.

4.2.17. Oxidative stability of nanoemulsion

The oxidative stability of fresh C-HP-US-StNE was measured using a Rancimat apparatus (Metrohm, model 743, Herisau, Switzerland) at 110 ℃ and 20 L/h air flow by measuring the volatile acid (free fatty acid) produced by radical chain reactions [57]. The amount of emulsion utilised for each expriment was 30 mL. The induction time was determined from triplicate analyses. The antioxidant activity index (AAI) was calculated from the measured induction time [32] by using the folowing formula **(Eq. 4.4)**

$$\mathrm{AAI} = \frac{\text{Induction times of carotenoids enriched nanoemulsion}}{\text{Induction times of untreated nanoemulsion}} \quad (4.4)$$

4.2.18. Effects of storage time and temperature on emulsion physical stability

Monitoring the degree of gravitational phase separation allowed for the determination of the emulsion stability index (ESI), which was calculated using the method developed by Karimi and Mohammadifar [27]. For this, 15 mL of freshly prepared emulsion was immediately put into a cylindrical glass tube, carefully capped the tube to overcome the evaporation loss, and then left undisturbed for 35 days at 6±2 ℃ and 25±3 ℃. At an interval of 7 days till 35 days of storage, relative rates of creaming were observed visually.

ESI can be expressed as followed (**Eq. 4.5**).

$$\mathrm{ESI}(\%) = \frac{H_E - (H_c + H_s)}{H_E} \times 10 \quad (4.5)$$

where H_E, H_c and H_s is the height of initial emulsion, cream layer, and sedimentation phase, respectively.

4.2.19. Experimental design for optimization

The designing of the experiments and optimization was performed using Response Surface Methodology (RSM). For modelling the experimental process, Box–Behnken

design (BBD) was used with homogenizing pressure, oil content, and surfactant as the three independent variables to predict the effect and optimize particle size of the nanoemulsion (dependent variable). A total of 17 experimental runs were carried out. The predicted model was fitted to a second-order quadratic polynomial. Design-Expert Version 13 (Stat-Ease) was used for the experiment design.

The experiment variables, given in **Table 4.2,** were coded according to **Eq. 4.6** [56]

$$y_j = \frac{Y_j - Y_{j0}}{\Delta Y_j} \quad (4.6)$$

where 'Y_j' and 'y_j' indicates the actual and coded values of the 'j' experimental variable, Y_{j0} is the real value of the 'j' experimental variable at mid (central) point, and ΔY_j is the step change of the dimensionless value.

Table 4.2. Real and coded values of the independent parameters for development of StNPs.

Experimental Variables	Code	Coded levels		
		-1	**0**	**+1**
High pressure (bar)	A	100	300	500
Oil content (%, ml/100 ml)	B	1	5.5	10
Surfactant (%, g/100 ml)	C	1	3	5

4.2.20. Optimization

Optimization of nanoemulsion synthesis was performed by setting the desired goal of output parameters and optimization was performed based on higher value of desirability [10] as mentioned in **Chapter 3**.

4.2.21. Methods adopted to obtain the thermal degradation kinetics

Coast–Redfern (modified), a model-free method used for simulating real data in a multi-step kinetics [38,40] was applied in this study of the kinetics of the NS and StNPs. To evaluate the kinetics of thermal decomposition of starch, the TGA data were used. The fundamental equation for the kinetics calculations is presented as follows (**Eq. 4.7**)

$$\frac{d\vartheta}{dt} = k.f(\vartheta) \quad (4.7)$$

Here, 'ϑ' and 'k' that represents the conversion rate and its rate constant(min^{-1}), can be calculated using the following **Eq. 4.8** and **Eq. 4.9,** respectively.

$$\vartheta = \frac{M_i - M_t}{M_i - M_f} \quad (4.8)$$

$$k = A \exp\left(-\frac{E_a}{RT}\right) \quad (4.9)$$

Where, $M_i, M_t,$ and M_f is the initial, at processing time 't', and the final (saturated) mass of the starch powder, respectively. Pre-exponential factor (min^{-1}) is denoted by A, while activation energy ($J.mol^{-1}.K^{-1}$) is represented by E_a. where, R = $8.314\ J.mol^{-1}.K^{-1}$ is the universal gas constant and T denotes the temperature (K).

The heating rate (β) of the starch during TGA can be expressed by **Eq. 4.10.**

$$\delta = \frac{dT}{dt} \tag{4.10}$$

Rate of reaction constant can be calculated with the help of modified Arrhenius equation and obtained by combining **Eq. 4.7, 4.9** and **4.10** and is represented by the following **Eq. 4.11.**

$$k(t) = \frac{A}{\delta} \exp\left(-\frac{E_a}{RT}\right) f(\vartheta) \tag{4.11}$$

where, $f(\vartheta)$ and $k(t)$ is the transition function and rate of reaction constant (min^{-1}), respectively.

During the treatment, temperature was varied from25 to 600 ℃, so it is assumed that pyrolysis is a non-isothermal process.

Integrating both to form the function with $g(\vartheta)$, as expressed by **Eq. 4.12** [49]**.**

$$g(\vartheta) = \int \frac{d\vartheta}{f(\vartheta)} = \frac{A}{\delta} \int \exp\left(-\frac{E_a}{RT}\right) f(\vartheta) \tag{4.12}$$

By using general Eyring–Polanyi equation, Gibbs free enthalpy of decomposition can be designated, which is expressed by **Eq. 4.13**.

$$k = \frac{k_b T}{h} \exp\left(-\frac{\Delta G}{RT}\right) \tag{4.13}$$

where, k_b and h is the Boltzmann constant and Planck constant and its value is $1.3806 \times 10^{-23}\ J.K^{-1}$ and $6.6261 \times 10^{-34}\ J.s$, respectively. ΔG is the Gibbs free energy ($J.mol^{-1}.K^{-1}$).

Enthalpy of the system can be estimated by combining **Eq. 4.9** and **4.13** and expressed as **Eq. 4.14.**

$$E = E_a = \Delta H + RT \tag{4.14}$$

Where, ΔH is the enthalpy ($J.mol^{-1}.K^{-1}$), and **Table 4.3** presents the $g(\vartheta)$ and $f(\vartheta)$ methods with appropriate mechanisms.

From the Gibbs function, entropy ($\Delta S, J.mol^{-1}.K^{-1}$) was calculated by the following **Eq. 4.15.**

$$\Delta S = \frac{\Delta H - \Delta G}{T} \tag{4.15}$$

Table 4.3. g(ϑ) and f(ϑ) Algebraic expressions functions for Kinetics modelling mechanism of the Coats–Redfern (modified) [49].

Mechanism	**g(ϑ)**	**f(ϑ)**	**Model name its code**
Random nucleation and growth	$\sqrt{(-\ln(1-\vartheta)}$	$2(1-\vartheta)\sqrt{(-\ln(1-\vartheta)}$	A_2
Random nucleation and growth	$\sqrt[3]{(-\ln(1-\vartheta))}$	$3(1-\vartheta)(-\ln(1-\vartheta))^{2/3}$	A_3
Random nucleation and growth	$\sqrt[4]{(-\ln(1-\vartheta))}$	$4(1-\vartheta)(-\ln(1-\vartheta))^{3/4}$	A_4
Unidimensional contraction	ϑ	1	R_1
Spherical phase boundary	$\sqrt[3]{(1-\ln(1-\vartheta))}$	$3(1-\vartheta)^{2/3}$	R_3
One-dimensional diffusion	ϑ^2	$\frac{1}{2}(\vartheta)^{-1}$	D_1
Three-dimensional diffusion	$(1-\sqrt[3]{(1-\vartheta)})^2$	$\frac{3}{2}(1-(1-\vartheta)^{\frac{1}{3}})^{-1}(1-\vartheta)^{\frac{2}{3}}$	D_3
First order (Random nucleation with one nucleus on the individual particle)	$-1ln(1-\vartheta)$	$(1-\vartheta)$	F_1

Equilibrium constant (K_{eq}) was calculated using the Van't Hoff isotherm expressed as (**Eq. 4.16).**

$$K_{eq} = \exp^{(-\frac{\Delta G}{RT})} \quad (4.16)$$

From the adopted kinetic model, **Eq. 4.12** was rearranged, and parameters E_a and A were determined by plotting the graphs obtained by **Eq. 4.17.**

$$\ln(\frac{g(\vartheta)}{T^2}) = \ln(\frac{AR}{\delta E_a}(1-\frac{2RT_{max}}{E_a})) - \frac{E_a}{RT} \quad (4.17)$$

4.2.22. Hydroxyl groups estimation of StNPs using TGA

To determine the quantity of hydroxyl group on surface area of a native starch and StNPs molecule, the following formula was used (**Eq. 4.18**) [49].

$$n_{OH}(C_6H_{10}O_5)_n = 2n_{H_2O} = \frac{2(ML(T_0)-ML(T_{final}))}{100M_{OH}} \quad (4.18)$$

where, $(ML(T_0) - ML(T_{final}))$ is the starch mass loss in % in the temperature range of $(T_0 - T_{final})$; M_{OH} and M_{H_2O} is the molar mass of hydroxyl group and water, and its value used was 17.008 g. mol^{-1} and 18.015 g. mol^{-1}, respectively.

4.3. Results and Discussion

4.3.1. Distribution pattern of particle size

Increase in ultrasound treatment time reduced the average particle size of starch granules in aqueous medium. As shown in **Fig. 4.1a**, a continuous decrease in the particle size up to 340 nm after 90 min of US was observed, which became less sharp after 60 min of treatment. PDI continuously decreased up to 90 min reaching 0.22 value, and thereafter a sharp increase was observed. The sharp increase in PDI value after 90 min may be due to re-agglomeration of the nanoparticles [42,59].

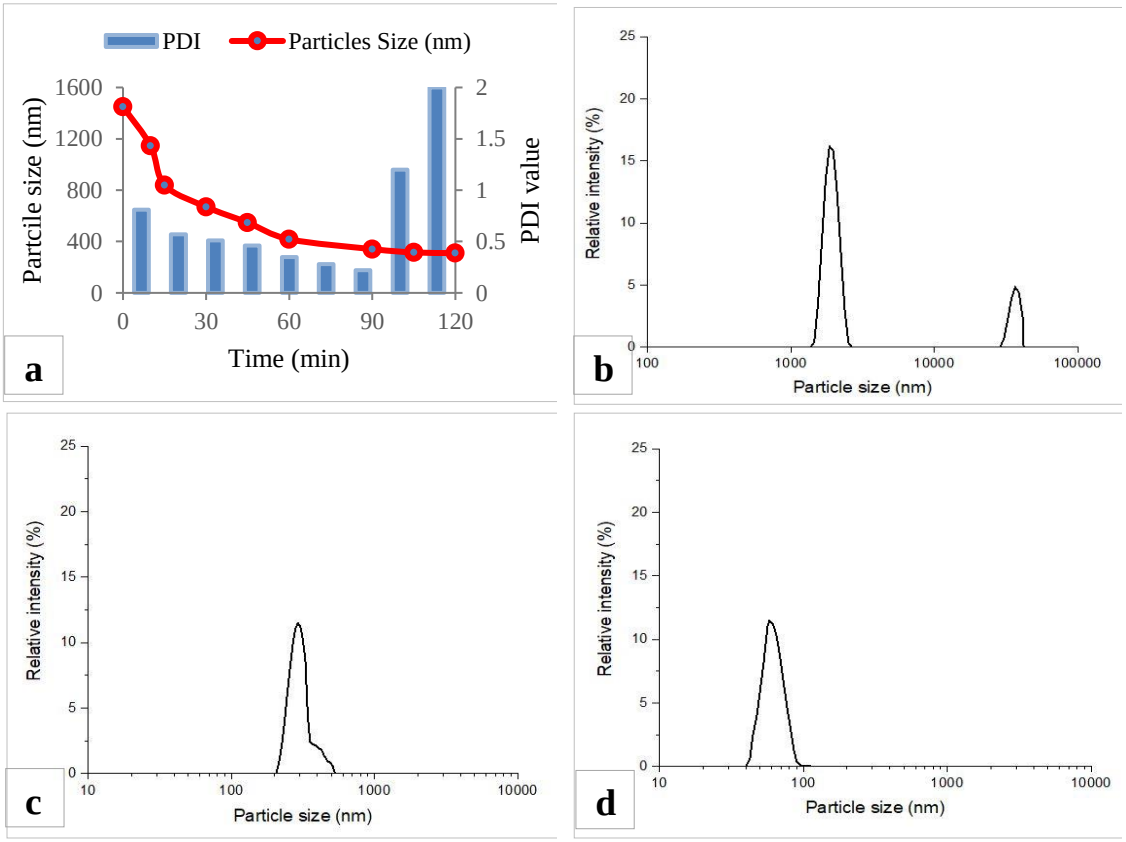

Fig. 4.1. (a) Effect of ultasonication treatment time on particle size and PDI value; Particle size distribution of: (b) NS, (c) US-StNP, and (d) HP-US-StNP.

Fig. 4.1 represents the particle size distribution of NS (**Fig. 4.1b**), US-StNP **(Fig. 4.1c),** and HP-US-StNP treatment **(Fig. 4.1d).** Native starch mostly contained the microparticles, showing bi-modal distribution of size (1.2-1.5 µm and 5-7 µm) **(Fig. 4.1b**), but after ultrasonication for 90 min, particles were completely transformed into nanoparticles (230-510 nm) and exhibited bi-modal distribution **(Fig. 4.1c).** When energy is supplied to the starch solution in the form of ultrasound, the applied energy gets transferred to starch particles by acoustic cavitation, and during the cavitation process bubbles generated on implosion create micro-turbulence with velocities greater than 100

m/s that causes vigorous collision among particles. This causes severe disintegration of the starch granules. Boufi et al. [4] observed size reduction of starch particles up to 40 nm after 75 min of US treatment using water-isoprene as solvent. In our study, although treatment time was quite high (90 min), there was less effect on size reduction, which may be due to the use of 100% water as solvent **(Fig. 4.1c)**. Kim, et al. [29] observed a bi-modal distribution of starch nanoparticles treated by US at low isothermal temperature. The bi-modal distribution may be related to distance dependency of US power intensity on the particles from the horn.

When the US treated starch was subjected to HPH at around 300 bar pressure, nanoparticles were effectively fragmented to smaller nanoparticles **(Fig. 4.1d**) varying in size from 38-96 nm. Liu et al. [37] were able to reduce particle size of starch from 3–6 μm to 10–20 nm using pressure of 207 MPa. In HPH, suspended fluid passes through the small nozzle at high velocities, as a result, the fluid experiences mechanical stress and turbulence that causes shearing and cavitation [15] and produces homogenous particles as compared to US **(Fig. 4.1d).** Amylopectin had a final z-average radius of gyration of about 20 nm after HPH treatment for eight cycles at 100 MPa or two cycles at 150 MPa, which was brought on by the midpoint scission mechanism [60].

4.3.2. Colour of StNPs

Starch powder of NS, US-StNP, HP-US-StNP and C-HP-US-StNP are shown in **Fig. 4.2**. Colour is an important parameter to evaluate the quality of starch powders. The

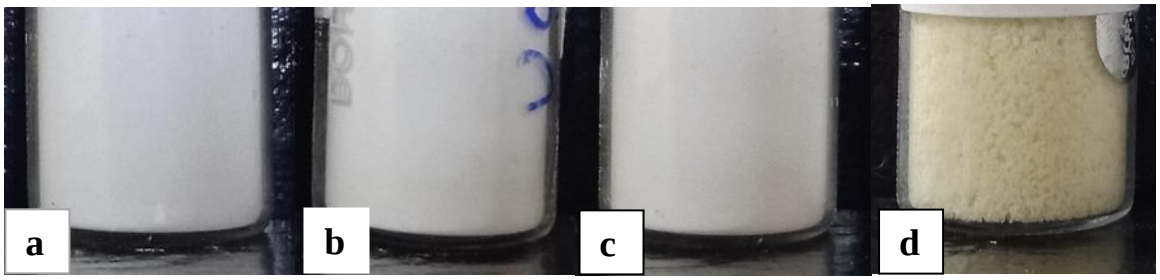

Fig. 4.2. Powder of (a) NS, (b) US-StNP, (c) HP-US-StNP, (d) C-HP-US-StNP.

variation in colour values of NS, US-StNP, HP-US-StNP and C-HP-US-StNP are tabulated in **Table 4.4.** The change in colour of L* value for US-StNP (97.85) was found to be non-significant but HP-US-StNP (96.09) was found to significantly differ with respect to NS (98.60). L* significantly decreased for C-HP-US-StNP (93.80) due to the carotenoid pigment. For all the starches, L* value greater than 90 confirms its purity [24]. The decrease in L* of US-StNP and HP-US-StNP may be due to the exposure of starch to

US and HPH treatment which led to rapid hydration of the granules. StNPs showed higher yellowness and redness than NS after the various treatments. This could be as a result of the starch molecules breaking down during the treatment, allowing some contaminants to link with them that lowers the whiteness and increases the redness and yellowness [24].

Table 4.4. Colour value of StNPs.

Sample ID	Colour value of different treated samples					
	L*	**a***	**b***	**X**	**Y**	**Z**
NS	98.60±0.44^{a}	-0.15±0.01^{a}	2.49±0.08^{b}	91.34±0.74^{a}	96.43±0.97^{a}	99.61±0.81^{a}
US-StNP	97.85±0.54^{a}	-0.19±0.02^{a}	1.656±0.94^{c}	89.54±0.67^{b}	94.55±0.95^{b}	98.91±0.81^{a}
HP-US-StNP	96.09±0.61^{b}	-0.10±0.01^{a}	2.40±0.08^{b}	85.50±0.62^{c}	90.23±0.85^{c}	93.26±0.78^{b}
C-HP-US-StNP	93.80±0.62^{c}	-2.13±0.14^{b}	15.75±0.57^{a}	79.32±0.71^{d}	84.80±0.85^{d}	70.12±0.88^{c}

4.3.3. Flow properties of StNPs

For these granular materials to flow, size of particle and its distribution pattern are crucial factors. The flowability of the powders according to HR value and repose angle is presented in **Table 4.5**. The HR value of starches slightly increased with treatment, and NS, US-StNP, and HP-US-StNP showed free flowing behaviour. HR value range for free-flowing powder was 1-1.25. HR of C-HP-US-StNP was 1.25, which is the critical value so it can be categorised as either free flowing or fairly free flowing properties. Similarly, based on repose angle, NS, US-StNP, and HP-US-StNP showed free flowing characteristic but C-HP-US-StNP exhibited fairly free flowing property. Due to the tight packing of the starch powders, there is limited space for molecular rearrangement or reorientation. As a result, the bulk density was only marginally greater than the aerated bulk, which produced a low HR value. According to Xinde et al. [61], HR is influenced by the size, shape, friction, and cohesive forces between particles.

Table 4.5. Flow properties of StNPs.

Samples ID	HR value	Flow ability based on HR	Repose angle	Flow ability based on Repose angle
NS	1.12±0.01	FF	33±0.09	FF
US-StNP	1.14±0.01	FF	34±0.08	FF
HP-US-StNP	1.17±0.01	FF	38±0.09	FF
C-HP-US-StNP	1.25±0.01	FF/FFF	46±0.10	FFF

* FF-Free Flowing; FFF- Fairly free flowing

Particles in NS were bigger in size, so gravity force was generally greater than inter-particle adhesive force that made it to flow easily, but for US-StNP and HP-US-StNP, too many small granules were produced that increased the contact area and as a result flow became difficult as compared to NS [61], even though particles were free flowing. For C-HP-US-StNP, oil coating of the starch nanoparticles surface hampered flow properties. Similar results for the emulsion of encapsulated beta carotenoids was reported by Xinde et al. [61]. It was found that the repose angle is the most appropriate index to represent the flowability of these powders because compaction or tapping during the testing process would not alter the particle characteristics [61].

4.3.4. Swelling power and solubility of StNPs

NS, US-StNP, HP-US-StNP, and C-HP-US-StNP exhibited swelling power values of 10.56, 17.98, 24.24 and 18.02 g/g and solubility values of 9.43, 14.28, 17.62 and 14.76%, respectively **(Fig. 4.3a** and **b).**

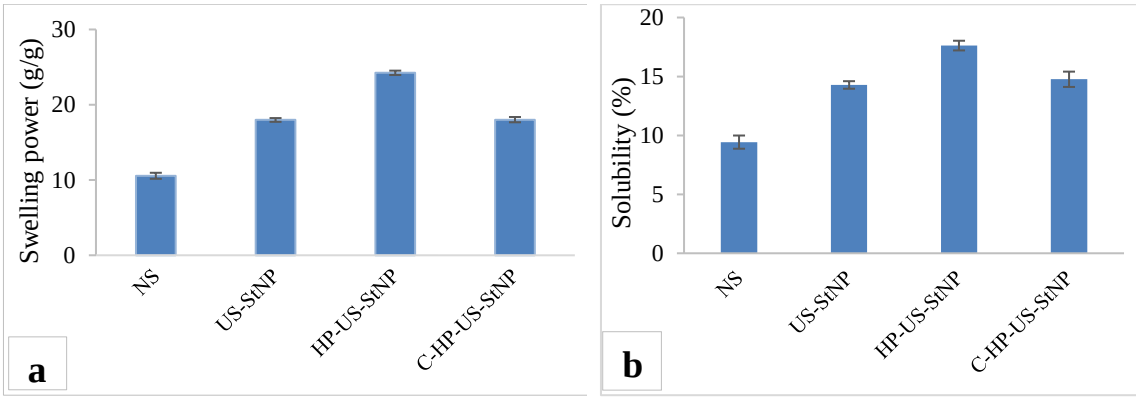

Fig 4.3. (a) Swelling power of StNPs, (b) Solubility (%) of StNPs

These values are in line with Kaur and Gill [28] and Liu et al. [37]. Elevation in swelling power after the treatments **(Fig. 4.3a)** indicated higher level of disorganization and disintegration of intermolecular bonds of the starch granules caused by extensive disruption of starch particle molecular structure and also binding of free hydroxyl groups of amylose and amylopectin to water molecules through hydrogen bonding [28]. The swelling power of C-HP-US-StNP decreased as oil coating was a hindrance. Both US and HPH-US treatments increased the solubility of starch **(Fig. 4.3b)** due to reduced particle size. Compared to its counterpart with tiny granule size, NS with big granule size demonstrated reduced solubility and swelling power. After both US [28] and HPH [19] treatments, the solubility of starch was increased**,** which supported the decrease in size of the starch particles. These treatments probably targeted the amorphous regions of starch

granules [19,28] that helped to release the amylose into the aqueous medium and increase solubility [28]. But after the addition of carotenoids-enriched oil, the solubility of the starch powder decreased as the granules were coated with the oil, which was confirmed by SEM (**Fig. 4.5).** Probably, complex formation of amylose with oil reduced starch solubility [59].

4.3.5. FTIR absorbance of StNPs

In addition to identifying the novel functional groups created by starch modification, FTIR has been frequently employed to identify short-range structural change and detect solid and gas components during heat degradation [28,37]. NS, US-StNP, and HP-US-StNP showed characteristic peaks at 3351 to 3404 cm^{-1} (**Fig. 4.4a)**, which are associated with stretching of O-H bond. This bond got strengthened on ultrasonic processing but was weakened after HPH treatment, which clearly indicated that ultrasonic treatment provides more potential to the structure of starch particles to hold on bound water [28].

The lesser intensity of the peaks in HP-US-StNP may be because of the destroyed starch structure that reduced their short-range order [19]. C-HP-US-StNP showed very weak peak for this band, which may be due to the effects of oil and carotenoids on starch and complex formation of lipid and amylose. Slight difference in peak intensity was observed among the studied samples. Bands at 2928 to 1071 cm^{-1} are assigned to the C-H stretching of glucose unit and was strengthened by both US-StNP and HP-US-StNP but lessened in C-HP-US-StNP. Water in an amorphous zone is indicated by bands at 1642 to 1652 cm^{-1}. Other peaks at around at around 989 to 1019 cm^{-1}, 1153 to 1164 cm^{-1}, and 1453 to 1465 cm^{-1} are associated with the vibration of C-O-H, vibration of C-H and stretching of C-H, respectively. Additionally, the peaks that emerged between 571 and 579 cm^{-1}, 761 and 768 cm^{-1}, and 923 and 936 cm^{-1} might be connected to anhydrous glucose ring stretching vibrations [28].

It has been reported that the characteristic peaks in FTIR spectrum are associated with the short-range order of starch chains. For example, absorbance ratio of 1047/1022 and 1022/995 indicates the short-range crystallinity and index of double helical structure order, respectively and lower 1047/1022 cm^{-1} ratio implies the lower value of short-range crystallinity, and higher value of 1022/995 cm^{-1} ratio means lower level of double helices [9,47]. For NS, ratio of 1047/1022 and 1022/995 were higher than 1 and lower than 1, respectively, which were in line with reported findings [28]. As shown in Fig. 4.4b, the 1047/1022 ratio increased on US treatment which may be associated with the increase in

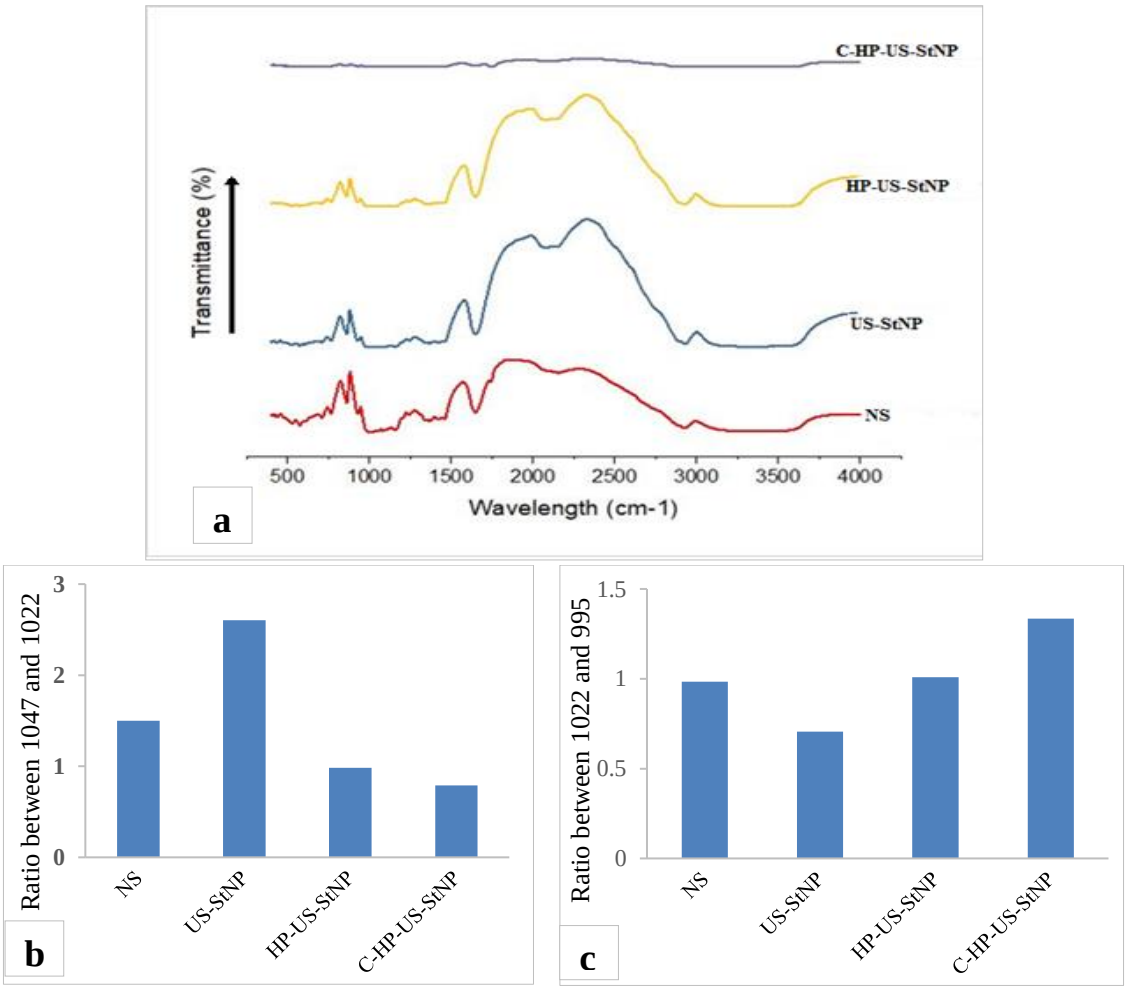

Fig 4.4. (a) FTIR absorbance spectra of starches samples; (b) Relation between 1047 and 1022 cm^{-1} brands, (c) Relation between 1022 and 995 cm^{-1} bands.

small crystals [28], but the ratio decreased significantly after HPH which may be because of high pressure on crystallites. These results support the XRD results **(Fig. 4.5).** The absorbance ratio of 1022/995 increased with US and HPH treatment (**Fig. 4.4c**), which suggested that US and HPH destroyed starch structure (also supported by swelling power values), and reduced their short-range order [19]. For C-HP-US-StNP, significantly higher 1022/995 was observed which indicated the severity of disorganized starch structure due to the formation of lipid-amylose complex.

4.3.6. Powder XRD analysis of StNPs

The crystalline characteristics of the treated starch granule in comparison to the native starch were determined using X-ray powder diffraction investigations, and the XRD diffractograms of all starches are presented in **Fig 4.5.** NS exhibited 2θ peaks of A-type pattern at about 15°, 17°,18° and 23.5° [9], indicating its semi-crystalline properties. A low intensity V-type peak was observed around 20° [4], which may be due to the formation

of amylose-lipid complex during the starch manufacturing process, as NS contained 0.26% oil. US and HPH treatments caused reduction in peak intensities and the effect of HPH was severe, but the peak for V-type pattern however, was not much affected [21].

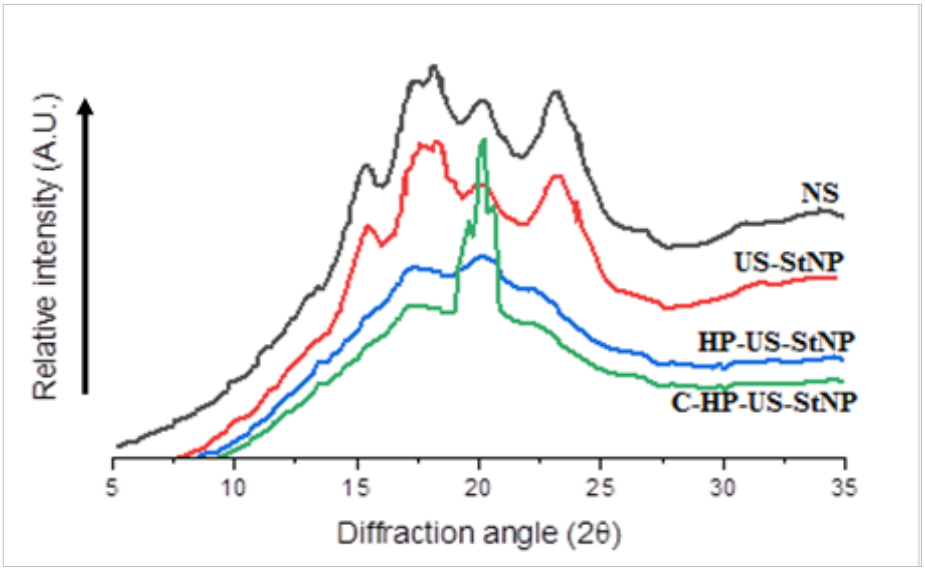

Fig 4.5. X-ray powder diffraction curve of different starch samples.

Ultrasonication reduces the crystallinity of corn starch because of the destruction of crystalline structure and weakened strong crystalline regions [4]. HPH generates tiny particles that further reduce crystallinity [2]. After the treatment with oil, significant loss of A-type crystallinity was observed [37] along with significant increase in V-type structure, probably due to the oil present [59].

4.3.7. Morphological studies

Microstructure of the native and treated starches was analysed using scanning electron microscope (SEM). SEM micrographs of NS, US-StNP, HP-US-StNP**,** and C-HP-US-StNP revealed the effect of treatment **(Fig. 4.6)**. Kaur and Gill [28] mentioned that maize starch is more treatment sensitive as compared to wheat, rice, and barley. The creation and explosion of cavitation bubbles during the US process results in significant pressure gradients, high local liquid layer velocities, and the thermal, mechanical, and chemical impact that it creates shatter particles, break polymer strands and reduce particle size [28]. Similarly due to the high pressure, solid particles pass through the small nozzle and generate shear force and high temperature and as a result reduction in size takes place [19,37]. All samples showed polyhedral granules **(Fig. 4.6a-f),** and US and HPH treatments caused reduction in granule size. Moreover, HP-US-StNP particles **(Fig 4.6e** and **4.6f)** were more uniform in size than US **(Fig 4.6c** and **4.6d)**,

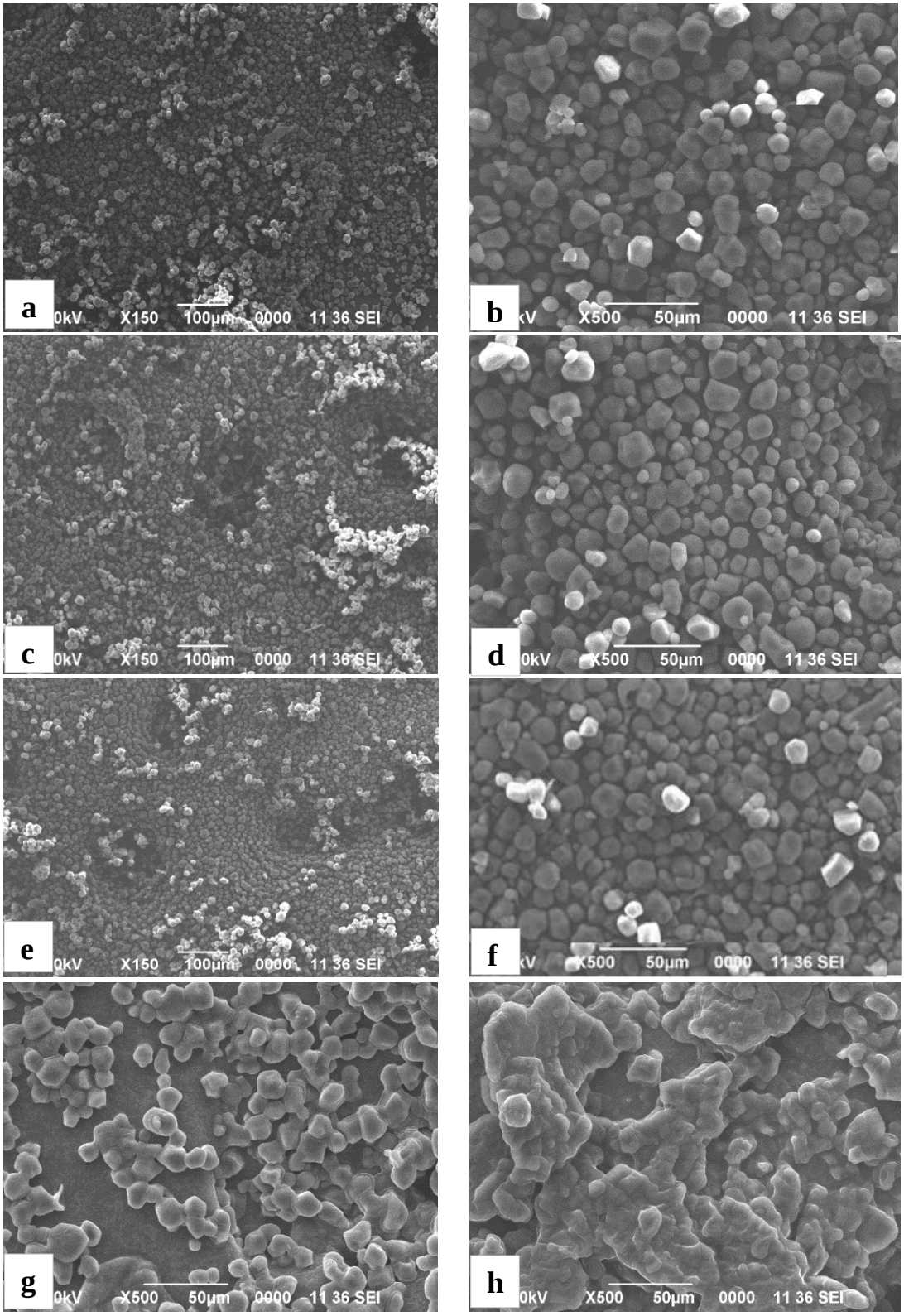

Fig. 4.6. Morphological structure of different starche samples: (a) NS (150X), (b) NS (500X), (c) US-StNP starch (150X), (d) US-StNP (500X), (e) HP-US-StNP (150X), (f) HP-US-StNP (500X), (g) C-HP-US-StNP (500X) and (h) Carotenoids starch (double oil amount) (500X).

this may be due to the use of probe ultra-sonication system where the concentric intensity of power was observed around the probe i.e., particles around the probe/horn are more affected as compared to the distant particles. After the US and HPH treatment, the water holding capacity of the starch nanoparticles increased as compared to NS, which was indicated by the opaque particle surface in **Fig. 4.6c-f** [30]. For C-HP-US-StNP, particles were completely covered with oil, but the particle size was well defined **(Fig. 4.6g),** indicating good flow properties **(Table 4.5)**. When the oil content was doubled, starch particles formed lumps **(Fig. 4.6h**), indicating poor flow ability.

US and HPH treatments brought homogeneity in the particles in this order: HP-US-StNP > US-StNP > NS. Kaur and Gill [28] observed smooth surface after ultrasonication treatment and Guo et al. [19] found smoother surface in HPH treated starch powder as compared to untreated one.

4.3.8. Rheological properties

It was observed that irrespective of the type of starch nanoparticle, 1 % starch suspension was a thin liquid that flowed easily, while 5 % suspension behaved like a gel **(Fig. 4.7**).

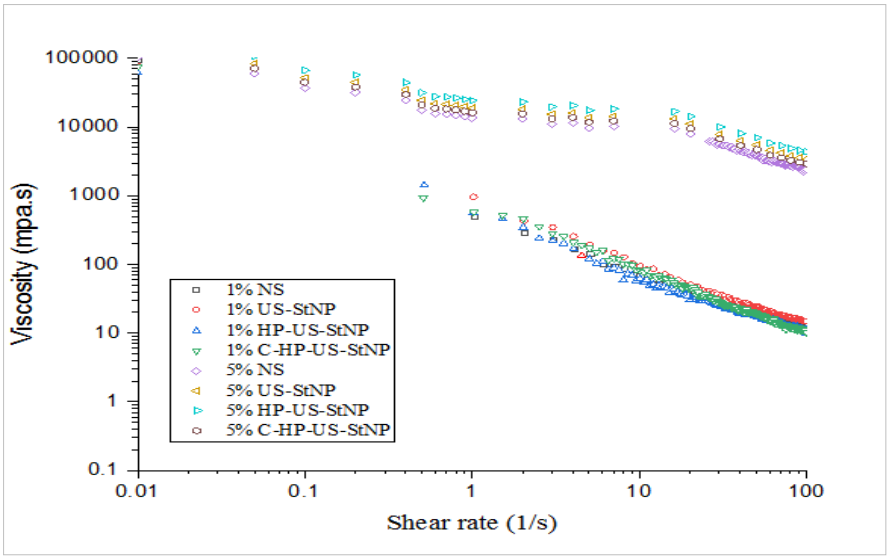

Fig. 4.7. Static rheological properties of 1 % and 5 % starch sample suspensions.

Liquid like behaviour of 1% starch suspension may be due to the primary and secondary electro-viscous effects between two particles. These effects occur due to the electrostatic repulsion within the electrical double layer of the particle and the fluid and due to the overlapping of double layers [48]. But at 5 % concentration, the gel-like behaviour of starch suspension indicates the formation of a network possibly due to strong

hydrogen bonding between the particles [48]. From **Fig. 4.7**, it was observed that there was similarity in the rheological behaviour of US-StNP, HP-US-StNP for both 1 and 5% suspensions. A slight increase in apparent viscosity after US treatment was observed which may be due to lesser degree of homogeneity (**Fig 4.6c** and **4.6d**), as hydrodynamic stresses depend on the shape and particle orientation during shear flow [37,48]. C-HP-US-StNP showed lower viscosity as compared to US and HPH that can be attributed to the oil present on the surface of starch.

4.3.9. DSC thermograms of StNPs

Melting temperature of starches can differ by 50 ℃ and depends on moisture content, amylose/amylopectin ratio, composition, and their botanical origin [28,33,38]. In this study, two peaks were observed. Lecorre et al. [33] reported that at intermediate water content (30–60%), a rise in temperature of starch sample leads to the emergence of two endothermic peaks. Researchers have given different explanations for the two peaks [33,38]. Briefly, in the sealed system, Liu et al. [38] noted two decomposition temperatures. They stated that the second peak at a higher temperature involved the disintegration of the glucose ring, whereas the first peak at a lower temperature showed long chain scission.

One researcher suggested that when the starch is dispersed in excess amount of water, water was absorbed by amorphous structure and expands and cross-links with semi-crystalline structures and form amorphous backbone resulting a loss of crystallinity. But when water becomes deficient for complete swelling, some crystalline structures still remain to melt and as a result melting is completed at higher temperature and therefore, there is an appearance of a second peak [13]. Another explanation is that the first peak causes the least stable crystallites to melt at low temperature, followed by a second melting peak at a higher temperature for the remaining stable crystallites [17]. Lecorre et al. [33] suggested that the multiple melting transition profiles were due to partial melting followed by recrystallization and final melting due to the lipid amylose complex. According to Lecorre et al. [33], the profile of several melting transitions was caused by partial melting, succeeded by recrystallization and ultimate melting caused by the lipid amylose complex.

The onset melting temperature of the first peak of US-StNP was around 40.8-44 ^{o}C, which was slightly higher than NS (39-40.2 ^{o}C), but the peak temperature (at 63.9 ^{o}C) and melting range (46 ^{o}C) was much higher than that for NS (53.5 ^{o}C and 26.6 ^{o}C, respectively). Similarly, the melting temperature and peak range for the second peak of

the US-StNP (onset temperature 88.2 ℃ and peak temperature 100.98 ℃) was much higher than NS (onset temperature 66.2 ℃ and peak temperature 87.8 ℃) **(Fig. 4.8)**. This increase in temperature may be caused by the amorphous regions breaking down during ultrasonication and a slight rearranging of the starch chains [29], or the production of numerous stable granules that are only a few nanometers in size, as shown by morphological study (**Fig. 4.6**).

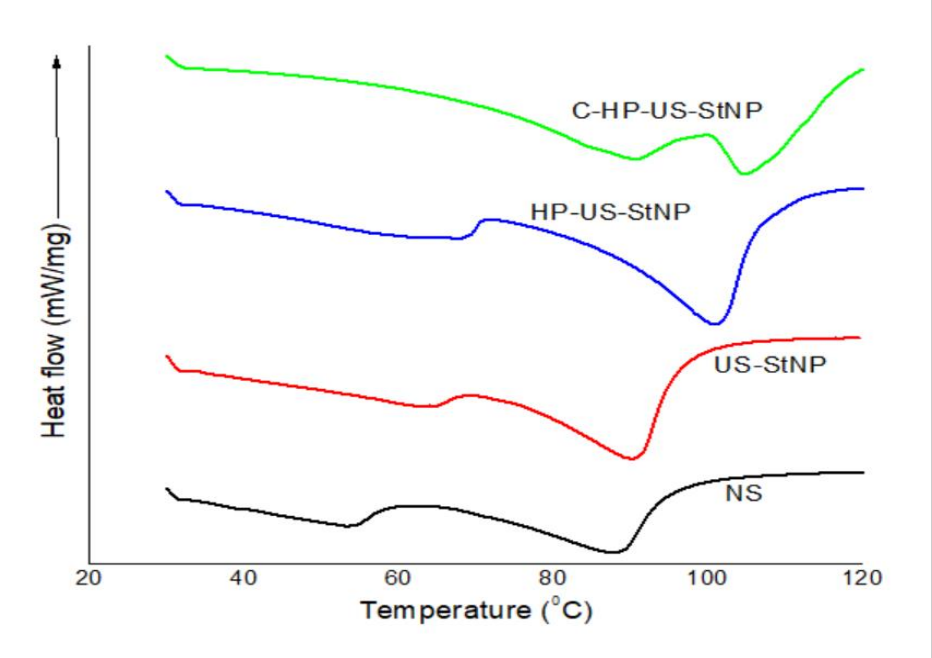

Fig. 4.8. DSC thermograms of starch samples.

The gelatinisation temperature of US-StNP was around 66 ℃. When the applied temperature is higher than the gelatinisation temperature, initiation of gelatinization takes place, which disrupts the intermolecular hydrogen bonds that maintain the structural integrity of starch molecules. Onset temperature and peak temperature **(Fig. 4.8)** of both peaks slightly increased in HP-US-StNP as compared to US-StNP, in agreement with Buckow et al. [5]. Perhaps, HPH treatment further disintegrated the amorphous regions [5,29] and produced more uniform small sized crystals [5]. For HP-US-StNP, the second peak increased notably which may be due to the formation of amylose-lipid complex [59].

For C-HP-US-StNP, a remarkable increase in both onset and peak temperatures for both peaks were seen **(Fig. 4.8)** because of the oil coating the granule surface (**Fig. 4.8**) that delayed gelatinization and induced amylose-lipid complex in the first peak [59], and the melting of the complex in the second peak.

4.3.10. TGA analysis of StNPs

When starch is heated, it decomposes following a complex process [29,49] **(Fig. 4.9)**.

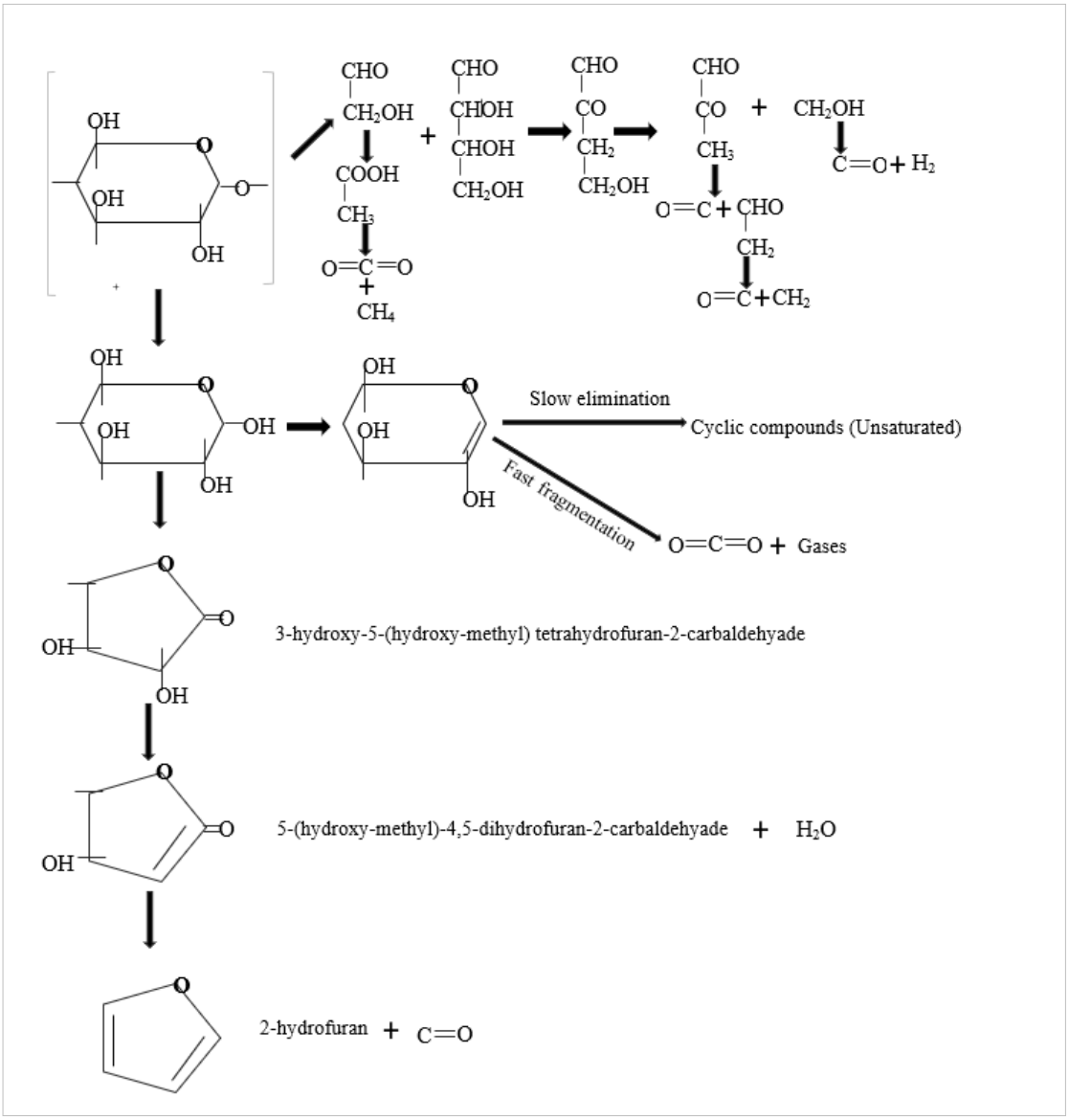

Fig. 4.9. Possible thermal degradation pathway of starch nanoparticles [49].

When starch is heated in the absence of oxygen i.e., in an inert chamber, pyrolysis to dextrins occur and the granular structure is destroyed, which allows its easy dispersion in cold water. Several steps are associated with pyrolysis: evaporation of water, degradation of hydroxyl groups, thermal decomposition of the organic compounds that are formed, and carbonization. Process temperature can go above 600 ^{o}C, but if the inert atmosphere is not maintained, ash formation takes place due to the presence of oxygen in the atmosphere. The obtained TGA graphs (loss of mass % vs temperature) of the StNP samples were used to determine the kinetics **(Fig. 4.10)**. Important challenges from a

scientific and industrial perspective are thermal deterioration and stability during processing [38]. The pyrolysis process of starch in an inert environment consists of several steps **(Fig. 4.9)**: (1) evaporation of the moisture from the starch, which depends on the water content adsorbed by starch; (2) thermal decomposition of the hydroxyl groups and organic compounds; and (3) carbonization. Diffraction patterns at about $180\ ^{o}\mathrm{C}$ are less sharp and at around $210-230\ ^{o}\mathrm{C}$, birefringence of molecules is destroyed, and amorphous regions are produced. A shown in **Fig. 4.10**, two major stages of decomposition for NS, US-StNP, and HP-US-StNP and three major stages for C-HP-US-StNP were observed during TGA analysis. **Fig. 4.10.** It clearly shows that NS, US-StNP, and HP-US-StNP followed almost the same pattern with US-StNP and HP-US-StNP showing almost identical thermogravimetric behaviour, indicating to have similar thermal properties.

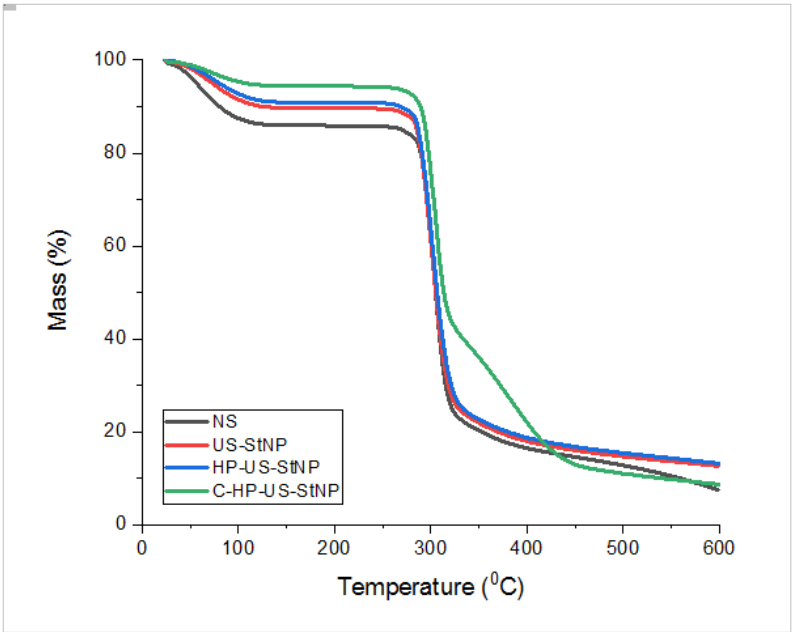

Fig. 4.10. TGA thermograms of starch particles.

The TGA mass loss graph for native and StNPs were different, may be because of the differences in crystalline and amorphous regions of the starch, the granule/ particle size, and different composition (carotenoids) especially of C-HP-US-StNP [38,49]. As shown in **Fig. 4.10,** the evaporation of water (initial stage of TGA curve) from NS was higher as compared to US-StNPs and HP-US-StNPs; the physical modification such as UST and HPH possibly caused the change in reactivity of starch due to the breakdown of functional groups [35,44]. In addition, these physical modifications reduced the granule size to nanoscale, which raised the density of hydroxyl groups at the surface of StNPs that increased the water holding area [44], and as a result, lower rate of water evaporation from

the StNPs occurred. With increasing temperature, the decomposition of StNPs decreased, which may be due the formation of uniform small particle size. Maximum mass loss was observed in the range of $280 - 320\ ^{o}$C for all the StNPs except C-HP-US-StNP, as also observed by Pigłowska et al. [49] for starch powder.

The decomposition behaviour of C-HP-US-StNP was different which may be due to the externally added oil and the formation of a stable amylose-oil complex [33,38]. According to literature reports, thermal transition of starches occurs in many stages, but major losses occur during the second stage [49] (approximately 90%), which is the main focus of this study.

4.3.11. Thermal decomposition Kinetics of starch samples

Decomposition kinetics of NS and StNPs was obtained according to **Eq. (4.17),** linear graphs were plotted between $\ln\left(\frac{g(\vartheta)}{T^2}\right)$ vs $\ln\ (\frac{1}{T})$ and the associated parameters were determined.

Table 4.6. Linear fit of plots for kinetics modelling of Coast–Redfern (modified).

Mechanism Code	NS (R^2)	US-StNP (R^2)	HP- US-StNP (R^2)	C- HP- US-StNP (R^2)
A_2	0.9501	0.9544	0.9589	0.9266
A_3	0.9419	0.9474	0.9526	0.9125
A_4	0.9316	0.9387	0.9448	0.9004
R_1	0.9192	0.913	0.9091	0.9001
R_3	0.8859	0.9415	0.9516	0.8810
D_1	0.9269	0.9048	0.9175	0.9068
D_3	0.9508	0.949	0.9529	0.9265
F_1	0.9615	0.9601	0.9641	0.9312

The thermal decomposition of starch is mainly connected to A_2, A_3, A_4, R_1, R_3, D_1, D_3, and F_1 models and these models were used to understand the kinetics process [49]. For NS and all StNPs, the best correlation/ prediction (highest $R^2 > 0.9312$) **(Table 4.6)** was observed for model ' F_1 ' and was best suited to explain the thermal degradation of StNPs. The F_1 model was therefore adopted for the remaining calculations. From the **Eq. 4.17,** E_a and A parameter values were determined and other thermodynamics parameters like ΔS, ΔG, ΔH, k, and K_{eq} were determined using **Eq. (13-16)**.

These parameters are generally associated with major mass loss (second stage) of the TGA graphs, i.e., in the region of $\pm\ 280 - 320\ ^{o}C$. A_2, A_3, A_4, R_1, R_3, D_1, D_3, and F_1 models were adopted in **Fig. 4.11a-d** to develop linear graphs for NS, US-StNP, HP-US-StNP and C-HP-US-StNP, respectively by plotting $\ln\left(\frac{g(\vartheta)}{T^2}\right)$ vs $\ln\left(\frac{1}{T}\right)$. **Table 4.7** represents the degradation kinetics and the thermodynamic parameters of StNP decomposition for the best model. The enthalpy (ΔH) value was found to be 139.050, 143.265, 144.496 and 157.652 kJ/mol for NS, US-StNP, HP-US-StNP and C-HP-US-StNP, respectively **(Table 4.7).**

Table 4.7. Estimation of the kinetic and thermodynamic parameters of StNPs.

Parameters	**NS**	**US-StNP**	**HP-US-StNP**	**C-HP-US-StNP**
Linear regression equation	-17303x + 16.831	-17810x + 17.720	-17959x + 17.910	-19543x + 20.142
R^2	0.965	0.960	0.964	0.931
E_a (KJ. mol^{-1})	143.857	148.072	149.311	162.481
A (min^{-1})	$3.923X10^{12}$	$9.891X10^{12}$	$1.194X10^{13}$	$1.200X10^{14}$
ln(A)	28.997	29.922	30.111	32.418
k (min^{-1})	0.018	0.017	0.018	0.021
ΔG (KJ.mol^{-1})	165.828	165.991	166.145	165.819
ΔH (KJ.mol^{-1})	139.050	143.265	144.496	157.652
ΔS (J.mol^{-1})	-46.401	-39.379	-37.458	-14.078
K_{eq} (-)	$2.284X10^{-15}$	$2.210X10^{-15}$	$2.263X10^{-15}$	$1.942X10^{-15}$

For all the StNPs, positive ΔH was observed which implied the endothermic nature of the process, and was also confirmed from DSC data. The ΔH value for US-StNP and HP-US-StNP was higher as compared to NS which may be due to the absorption of large quantity of ultrasonic energy, however, there was no notable change between US-StNP and HP-US-StNP. Use of high pressure, however, did not cause noteworthy changes in the double helix as compared to UST treatment. The ΔH value for C-HP-US-StNP was higher as compared to HP-US-StNP, US-StNP and NS and this remarkable shift in enthalpy may be due to the combined effect of treatment and external oil addition, which changed the helices in both amorphous and crystalline regions [44,59]. Crystalline regions are systematic arrangement of molecules, whereas amorphous regions are random arrangements.

It was mentioned that the thermal stability of C-HP-StNP was improved by replacing the hydroxyl groups of starch with alkyl ether groups [38]. In this study, ΔG value of NS, US-StNP, HP-US-StNP and C-HP-US-StNP was found to be 165.828, 165.991, 166.1450 and 165.819 KJ/mole, respectively **(Table 4.7.),** which are supported by Pigłowska et al. [49]. The ΔG values were positive and much higher than zero, which implied the non-spontaneous nature of the reaction and an absolutely forced process. The ΔG value of HP-US-StNP was found to be slightly higher than US-StNp, NS and C-HP-US-StNP, which may be due to the smaller granule size of starch particles and the severe degradation of amorphous region.

The negative value of ΔS indicates the undesirable nature of the process, as the entropy is inversely related to degree of freedom. The transformation process that showed a decrease in entropy was against the natural process that moves naturally to a state of increased entropy. In this study, treatments given were found to decrease the degree of freedom **(Table 4.7)**. C-HP-US-StNP showed lowest degree of freedom, which may be due to the surface of the StNP molecules being covered by the oil molecules**.** The K_{eq} value was found to be small and lower than zero for NS and all StNPs, which indicated that the reaction was irreversible [49].

In TGA, the first stage of mass loss is mostly associated with the dehydration of the starch molecules. As shown in the thermograms in **Fig. 4.10**, major mass loss in all samples occurred during the second stage. The degradation reactions began at around 280 ℃, when the formation of ether fragments started because of the thermal condensation of -OH groups of StNP with the release of water molecules. Degradation of the glycosidic ring present in StNP or C=C bond formation from -OH groups in the glycosidic ring takes place, while dehydration occurs in its neighbourhood [49]. At the same time, monosaccharide ring becomes damaged and terminal groups are formed by the aldehyde group. Aromatic rings with groups such as $–CH_2–$ or $–CH_2–O–CH_2–$ (specially benzene and furan structure) act as the main binders between aromatic rings that are formed when degradation temperature increases [40]. Generally, amorphous region develops at temperatures above 550-600 ℃, because of which mobility of ions is increased, which enhances the diffusion and thermo-diffusion of the process. In the third stage, slight mass loss occurs, which could be related to strong C–C bonds present in amorphous carbon [49]. This is because starch degradation reactions begin at around 280 ℃ and when the temperature of starch increases up to approximately 550 ℃, the aromatic compounds with

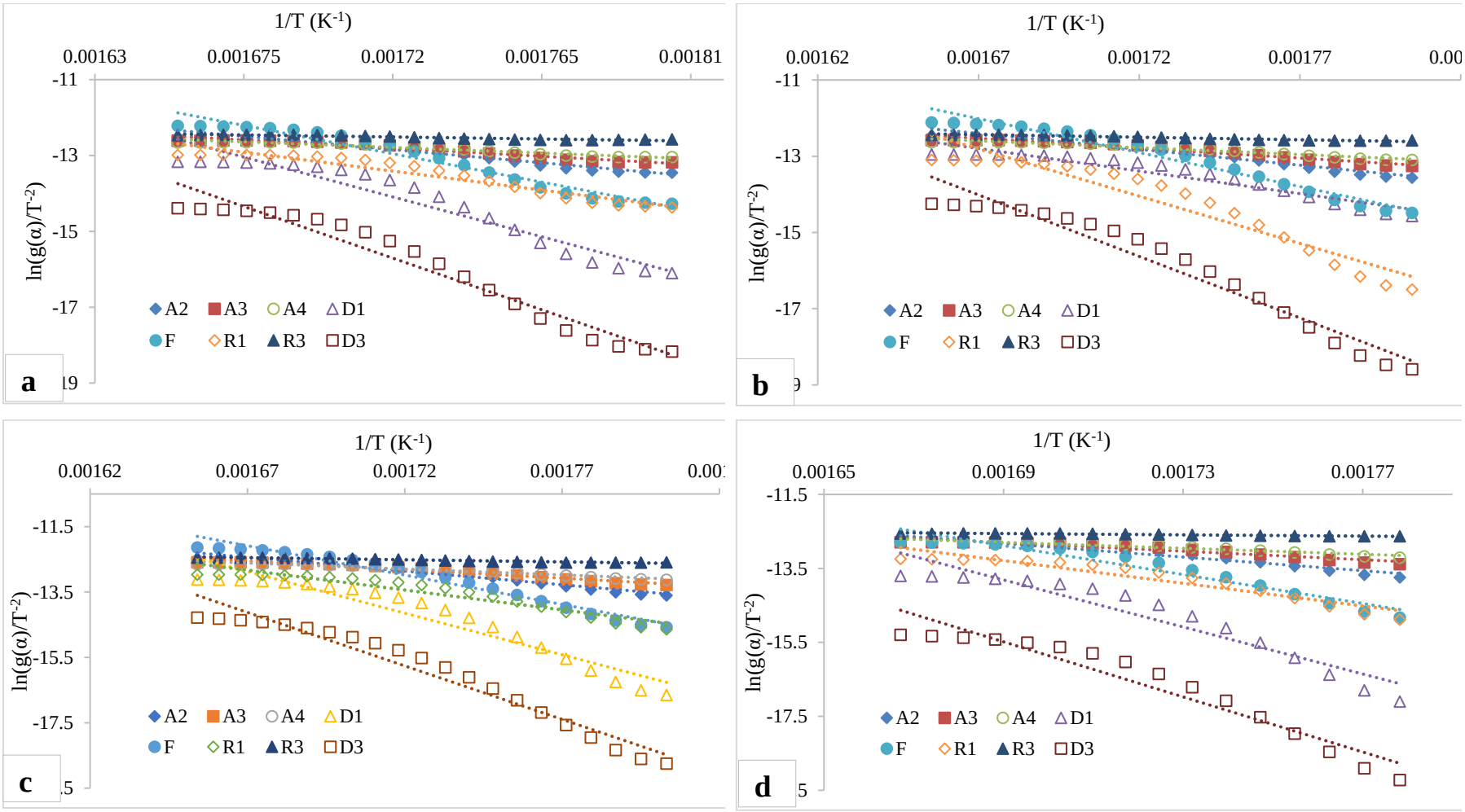

Fig. 4.11. Plot ln $(\frac{g(\alpha)}{T^{-2}})$ vs $\frac{1}{T}$ of (a) NS, (b) US-StNP, (c) HP-US-StNP, and (d) C-HP-US-StNP.

-CH_2- or –CH_2-O-CH_2 groups are formed, and their formation initiates the process for development of amorphous region [49]. The activation energy of NS, US-StNP, HP-US-StNP and C-HP-US-StNP was found to be 143.857, 148.072, 149.311 and 162.481 KJ/mol, respectively, which is in line with the investigation performed by Pigłowska et al. [49]. Some differences in the activation energy among the StNPs samples were observed, which may be related to modification treatments, low moisture content, or low carbon content [49]. So, NS degraded before other starches, followed by US-StNP, HP-US-StNP and C-HP-US-StNP. According to **Table 4.7,** decomposition energy of samples decreased in this order: C-HP-US-StNP > HP-US-StNP > US-StNP > NS. Thus, the most energy-consuming was carotenoids-enriched StNP and least energy-consuming was NS. This reason may be related to the small size of granules with more stable microstructures in US-StNP and HP-US-StNP. The formation of stable lipid-amylose complex in the carotenoids-enriched StNP required the maximum energy for decomposition. The maximum reaction rate constant value was for C-HP-US-StNP, and the lowest value was for US-StNP. During the cavitation process in homogenization, as the pressure increases, the covalent bonds between the macromolecules are ruptured and formation of new bonds are favoured that allow for increased stability [44]. In addition, **Fig. 4.11a-d** does not show any linear trend, which suggests multi-step degradation reactions for the NS and StNPs. The decomposition kinetics of NS and STNPs, the activation energy, and pre-exponential factor were determined in this study and the results agree with the literature reports [45].

4.3.12. Determination of hydroxyl groups in StNPs using second mass loss from TGA

As the major fraction of mass loss in TGA process occurred during the second stage, the total hydroxyl groups content was calculated from the entire second mass loss (**Table 4.8).** A proportion of total water strongly binds to specific hydroxyl groups in the polysaccharides, and when Braunauer-Emmett-Teller (BET) monolayer value is equivalent to moisture content then it is said to be stable in nature. If BET value is lower than the moisture content, there are chances of higher rate of oxidation and susceptibility to microorganisms [18]. It was noticed that only a few hydroxyl groups remained on the structure of StNP after the second mass loss step, which was also reported by Spychaj et al. [58].

As given in **Table 4.8**, content of hydroxyl groups on the surface of all starches varied between 1037.488 and 1307.742 mg/g, which confirmed their belonging to the carbohydrates category.

Table 4.8. Hydroxyl groups and physiosorbed water determination on the surface of starche samples

Starch	**NS**	**US-StNP**	**HP- US-StNP**	**C-HP- US-StNP**
Initial mass(mg)	16.501	16.502	16.502	16.504
Final mass(mg)	1.251	2.090	2.175	1.439
Whole mass loss (%)	92.47	87.333	86.816	91.278
Whole mass loss(g)	0.015	0.014	0.014	0.015
Mass loss associated with water release (%)	9.977	10.329	10.374	8.572
nH_2O (mg/g of starch) (physisorption)	99.788	103.290	103.740	85.720
nH_2O (mmol/g of starch)	5.539	5.734	5.758	4.757
Mass loss associated with hydroxyl groups release (%)	60.470	62.815	62.874	51.876
nOH (mol/g of starch)	0.071	0.075	0.077	0.061
nOH (mmol/g of starch)	71.012	75.072	76.889	61.009
nOH (mg/g of starch)	1207.568	1276.891	1307.742	1037.488

Amount of hydroxyl groups present in starch depends on the source, water content, and black carbon amount. Generally, carbohydrates contain 60–75 % of water, including the hydroxyl groups, and 25–40 % of black carbon. Hydroxyl groups present in corn, rice, potato and wheat starch amounts to 1078, 1023, 960, and 1015 mg OH per g starch [49]. He et al. [22] reported that cellulose contained about 1037 mg OH per gram of polymer. Similarly, 1078 mg OH per gram of corn starch was observed by Pigłowska et al. [49]. After the treatments, amount of OH groups increased from 1207.568 to 1276.891 and 1307.742 in US-StNP and HP-US-StNP samples, respectively, which may be due to the size reduction of starch from micro to nano size and due to the breakdown of functional groups [35,44]. Boufi et al. [4] also mentioned that the nano scale of the starch contained higher density of hydroxyl groups on the surface than the microparticles.

4.3.13. Properties of the Pickering emulsion stabilized with starch nanoparticles

4.3.13.1. Effect of high pressure on particle size of the nanoemulsion

Generally, up to 500 bar homogenization pressure is normally used in the industry [59], so in this study pressure range from 100 to 500 bar was selected for emulsion development. The effects of pressure on particles size of emulsion were not significant ($p=0.0535 > 0.05$ **(Table 4.9).** The particle size initially decreased as high pressure was

increased to approximately 310 bar **(Fig. 4.12a-d)** and then increased with further increase in pressure, while other parameters were kept constant. In HPH, breakdown of starch particles and droplets occur due to the combination of shearing, grinding, and cavitation [52], which reduces the particle size. Similar results were observed by several researchers such as Ding and Kan [15], Li et al. [36] and Romanski et al. [52]. Li et al. [36] reported that for the HPH, a pressure of 30 MPa was sufficient to significantly alter the chain length of starch (reduced the particle size), but further pressure increase had less of an impact. After 310 bar pressure, increase in particle size were observed, which may be because higher pressure causes partial geletinization of starch granules and consequent agglomeration because of resultant increase in temperature [19,59]. The irreversible agglomeration of starch nanoparticles is caused by van der Waals forces; ultrasonication treatment prior to HPH treatment is therefore helpful in reducing the severity of HPH treatment besides decreasing the size [52]. **Fig. 4.12g** shows that the effect of high pressure on size reduction was positive (reduction in particle size) around its central level but was negative beyond the central level. Guo et al., [19] reported that upto some pressure the size reduction of the particles take place but on further increase in pressure some ruptured starch granules that had slightly swollen surfaces had aggregated with other granules, and as a result increase in over all size occurred. Romanski et al. [52] investigated about the side effects of severe high-pressure treatment and observed that severe high pressure tend to irreversibly agglomerate starch nanoparticles. They also mentioned that this may be caused by attraction due to van der Waals forces between small particles which intensifies greatly as particles become smaller. Thus, prior to HPH treatment, ultrasonication treatment play a significant role in not only reducing particle size but also reducing the severity of HPH treatment.

4.3.13.2. Effect of oil content on particle size of nanoemulsion

In **Chapter 3**, it was already established that extracted CEOO was enriched in carotenoids and other bioactive compounds, so higher amount of oil in the emulsion is desirable. But as oil plays an important role on emulsion size, optimization of oil content in emulsion is crucial. Also, optimization of oil content in the emulsion is very important as emulsion formation of the enriched oil is desirable for wider food applications. As shown in **Fig. 4.12a** and **b** and **Fig. 4.12e** and **f**, the size of the emulsions was found to decrease with an increase in oil content up to 4.4 ml/100 mL, thereafter size increased with further increase in oil content.

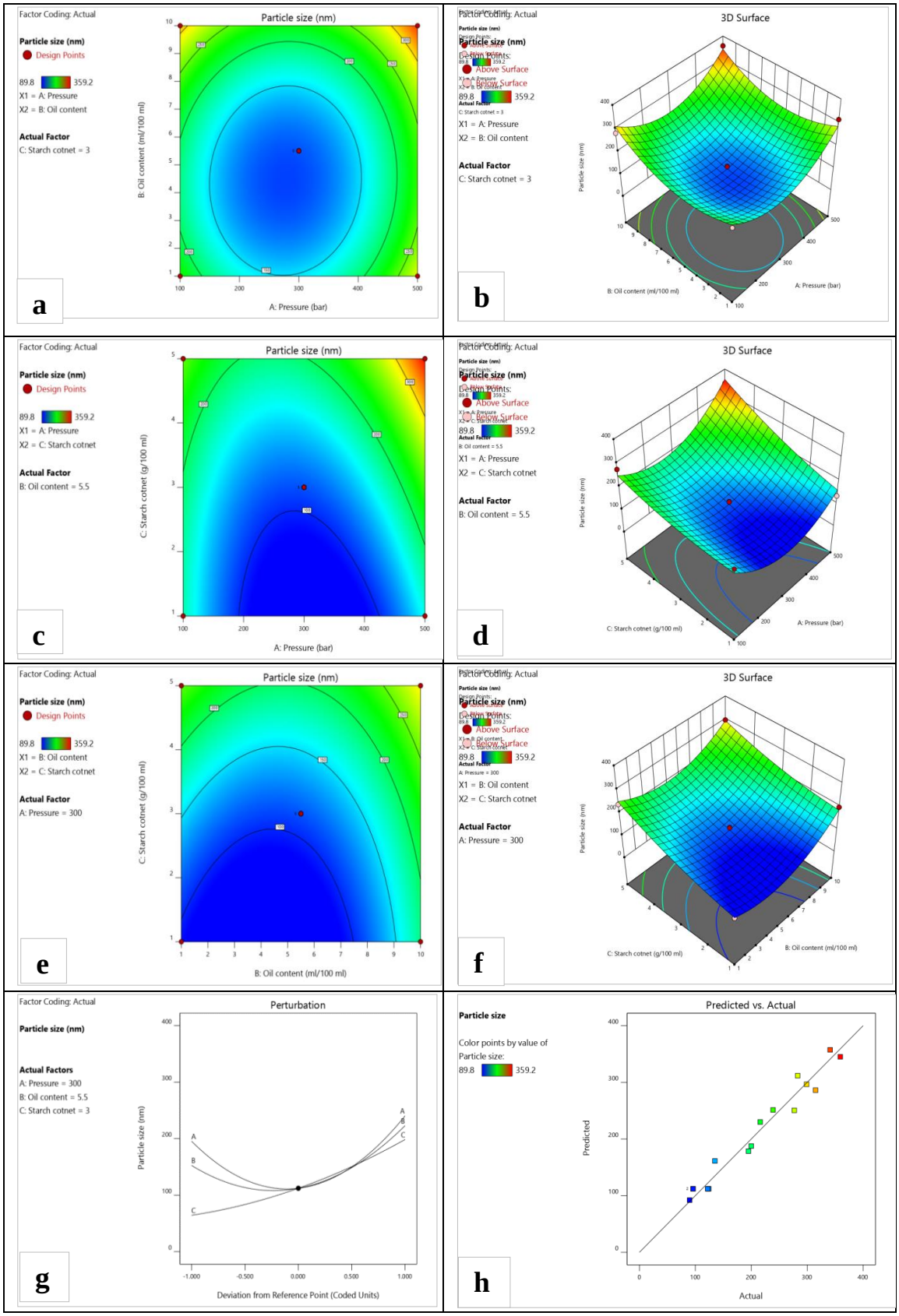

Fig. 4.12. Response surface plots showing the effects of parameters on particle size in nano emulsion preparation process. Parameters in (a) 2D contour plot between pressure and oil, (b) 3D contour plot between pressure and oil, (c) 2D contour plot between pressure and

surfactant, (d) 2D contour plot between pressure and surfactant, (e) 2D contour plot between pressure and oil, (f) 3D contour plot between pressure and oil, (g) Deviation from reference point, and (h) Predicted vs. actual data.

Generally, during HPH, starch molecules may absorb water and swell as temperature rises, but in this study the swelling process was hindered due to coating with oil [59]. Therefore, increase in oil content up to a certain level decreases the overall size of emulsion droplets but beyond the critical limit, no further disintegration occurs and an increase in size takes place probably because the excessive oil deposits as a thick layer on the surface [15]. Similar trend was observed by Asua, [3] and Ding and Kan, [15]. The overall effect of oil content on size reduction process was found significant ($p < 0.05$) **(Table 4.9).**

4.3.13.3. Effects of starch content on particle size of the nanoemulsion

Choi et al. [9] had reported about the significant effect on stability index of starch based emulsion with starch content up to 5 %. So, the range of starch to produce the nano emulsion was chosen between 1-5%. Emulsion size was seen to slightly decrease with an increase in starch content from 1 to 1.2g/100 mL (**Fig. 4.12c** and **d** & **Fig. 4.12e** and **f)** but thereafter a gradual increase in size was observed. Romanski et al. [52] reported that starch concentration above 2 % (w/w) restricted size reduction due to high viscosity and transition to non-Newtonian behaviour. After homogenization, when the amount of surfactant is insufficient to coat the whole surface area of the droplets, they aggregate with each other but when the amount become excess in oil, surfactant adheres to the droplets and form larger sized droplets [15].

4.3.13.4. Modelling and validation

The quadratic equation fitted with designed experimental data (BBD design) to explain the effect of input parameters is represented in **Eq. 4.19.**

$$\text{Particle size} = 112.52 + 22.28 \times A + 35.04 \times B + 66.96 \times C - 5.78 \times A \times B + 31.02 \times A \times C - 12.50 \times B \times C + 105.99 \times A^2 + 75.12 \times B^2 + 18.97 \times C^2 \quad (4.19)$$

As shown in **Fig. 4.12h**, there was a good correlation between the predicted values calculated by using the model equation and experimental values, which indicates the good fitting of the model. R^2 value was 0.9625. Lack of fit was found to be non-significant and the model was highly significant (0.0003), implying the validation of model.

Table 4.9. ANOVA table of nanoemulsion preparation process

Source	Sum of Squares	dF	Mean Square	F Value	p-value Prob > F	Remarks
Model	1.326E+005	9	14736.94	19.95	0.0003	Significant
A-Pressure	3969.40	1	3969.40	5.37	0.0535	
B-Oil content	9821.01	1	9821.01	13.30	0.0082	
C-Surfactant	35871.81	1	35871.81	48.56	0.0002	
AB	133.40	1	133.40	0.18	0.6836	
AC	3850.20	1	3850.20	5.21	0.0564	
BC	625.00	1	625.00	0.85	0.3883	
A^2	47300.55	1	47300.55	64.04	< 0.0001	
B^2	23756.90	1	23756.90	32.16	0.0008	
C^2	1514.41	1	1514.41	2.05	0.1953	
Residual	5170.65	7	738.66			
Lack of Fit	4275.36	3	1425.12	6.37	0.0529	Not significant
Pure Error	895.29	4	223.82			
Cor Total	1.378E+005	16				
R^2	0.9625					

4.3.13.5. Optimization

As shown in ANOVA table **(Table 4.9),** input parameters of oil content and starch content, with a probability value of 0.0082 and 0.0002, respectively were found to be the significant factors.

Table 4.10. Optimization conditions of carotenoid-enriched nanoemulsion

Pressure (bar)	Oil content (%, v/v)	Surfactant (g/100 ml)	Particle size (nm)	Desirability
310.806	4.400	1.156	59.058	1.000
302.104	3.855	1.269	62.033	1.000
283.802	3.420	1.159	62.475	1.000
288.271	4.961	1.303	65.531	1.000
314.074	3.250	1.333	66.416	1.000

Although input parameter of pressure was non-significant (p=0.0535>0.005), second order effect of pressure (A^2) and oil content (B^2) were found to be highly significant with p value <0.0001 and <0.0008, respectively. Optimized conditions consisting of 310.801 bar pressure, 4.400 ml/100 ml oil and 1.156 g/100 ml gave maximum desirability level of 1.0 **(Table 4.10).** At these conditions, predicted value of particle size was 59.058 nm whereas the optimized value was 61.25 nm.

4.3.14. Properties of starch-based nanoemulsion

Quality parameters of C-HP-US-StNE were compared with nanoemulsion developed using normal olive oil **(Table 4.11).**

Table 4.11. Biochemical properties of carotenoids enriched starch nanoemulsion

Parameters	**Nanoemulsion of normal olive oil**	**Carotenoids-enriched nanoemulsion**
Total phenolic content (mg GAE/100mL emulsion)	0.914±0.15	12.21±0.85
Carotenoids (µg/100mL emulsion)	8.21±0.59	24.254±0.87
β-carotene ((µg/100mL emulsion)	3.14±0.54	11.85±0.46
Antioxidant activity (ABTS assay)	15.8 ±2.5	27.6 ±3.5

As shown in the **Table 4.11,** total phenolic content in C-HP-US-StNE was 12.21 mg GAE/ 100 mL, which was 13.4 times higher than normal OO emulsion. Similarly, 24.254 µg/100ml of carotenoids content was observed in C-HP-US-StNE and its value increased approximately three times than the normal OO emulsion.

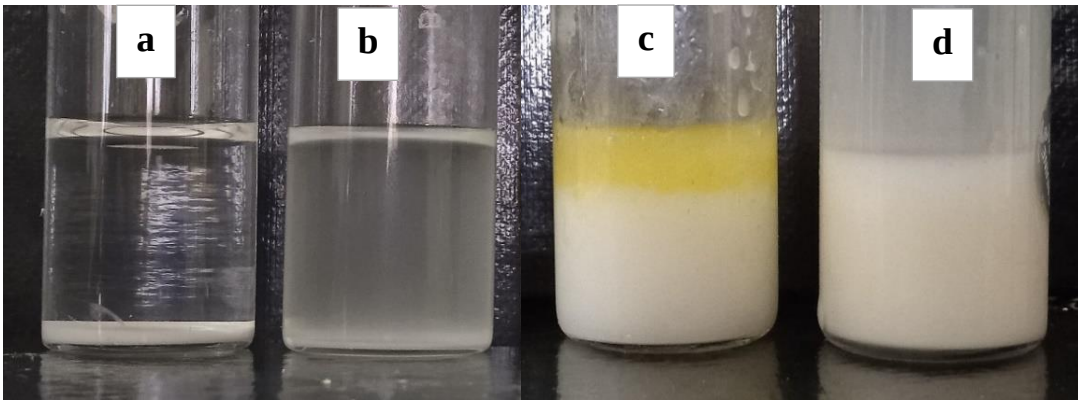

Fig. 4.13. Starch nanoparticles after 24 h storage at room temperature, (a) Native starch, (b) HPH starch nanoparticles, (c) Nanoemulsion without HPH, (d) HPH treated nanoemulsion.

Thus, significantly higher amount of total phenolic content and carotenoids, and greater antioxidant activity was seen in C-HP-US-StNE. These results highlight the positive effect of C-HP-US-StNE. The images of suspensions of NS, HP-US-StNP, and nanoemulsions with and without high pressure homogenization after 24 h of storage at room temperature are presented in **Fig. 4.13**.

4.3.15. Heat and freeze thaw stability of nanoemulsion

Emulsions developed with StNP were observed to produce a stable emulsion even after heating or freeze-thaw treatment **(Fig. 4.14).** Choi et al. [9] reported excellent freeze-thaw stability of the emulsion stabilized by starch on storage at -18 °C.

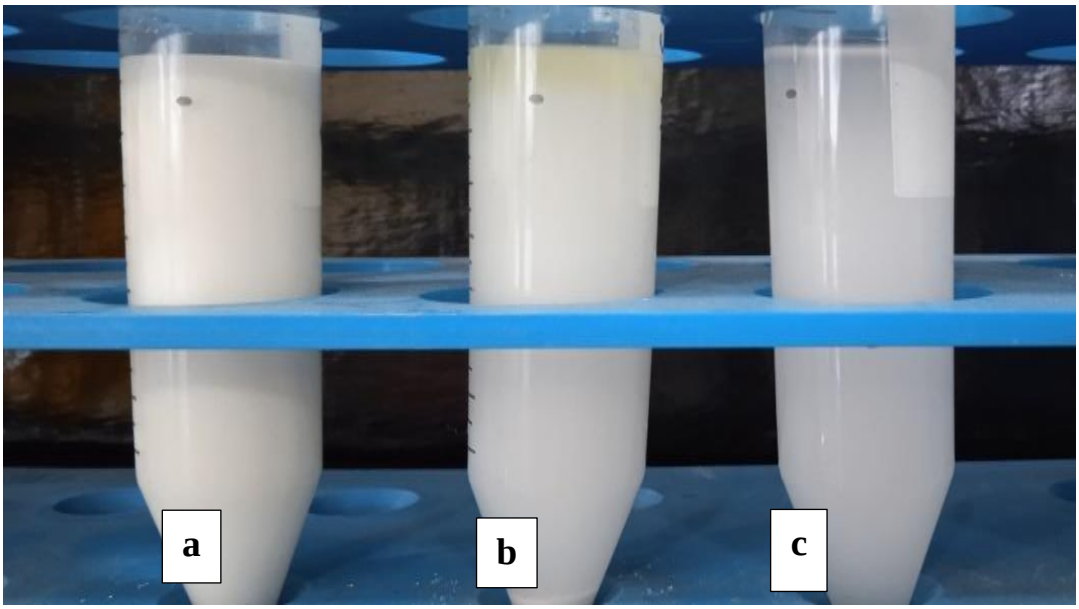

Fig. 4.14. Emulsion stability in (A) Fresh emulsion, (B) after heat treatment, and (C) after freeze-thaw treatment.

4.3.16. Effects of antioxidants on oxidative stability of nanoemulsion

The induction time and oxidative stability index of normal OO emulsion (without carotenoids) was 7.29 h and 13.28, respectively **(Table 4.12)**. The high induction time and oxidative stability is because olive oil predominantly has monounsaturated fatty acids along with high concentration of carotenoids and polyphenols [31]. Induction time of emulsions of corn oil, peanut oil, soyabean oil and sunflower oil ranges from 4.74-8.58 h [11].

Induction time and oxidative stability index of C-HP-US-StNE was 12.68 h and 22.18, respectively **(Table 4.12)** and the antioxidant activity index (AAI) value was around 1.74, supporting Daniela et al. [57] and Lante and Friso [31]. The significantly high

oxidative stability and antioxidant properties of C-HP-US-StNE may be due to greater quantity of polyphenols and carotenoids as compared to untreated olive oil (**Chapter 3).**

Table 4.12. Oxidative stability of nanoemulsion.

Sample	Induction time (h)	Oxidative Stability Index(h)	AAI
Normal emulsion	7.29 ± 0.42	13.28 ± 1.72	1.74
Carotenoids enrich emulsion	12.68 ± 0.87	22.18 ± 2.13	

4.3.17. Quality of nanoemeulsion on storage

4.3.17.1. Effect on antioxidant activity

The antioxidant activity of CEOO emulsion may be because of carotenoids (main portion was β-carotene), polyphenols, and anthocyanins present.

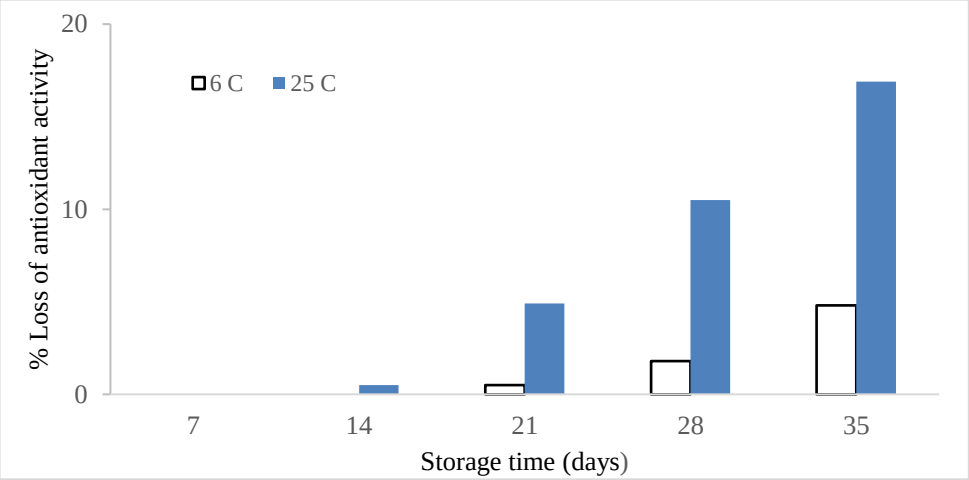

Fig. 4.15. Protective effect of nanoemulsion on antioxidant activity.

The antioxidant activity of the nanoemulsion that was developed using optimized condition was 28.8 % **(Fig. 4.15),** which after 21 days storage at 25 ℃ with an exposure to natural light decreased by 5.6 % and after 28 days reduced by 14.5 %. A non-significant reduction of 4.8% of the antioxidant activity was observed after 5 weeks of storage at 5 ℃ (in dark). In comparison, Ruiz-Montañez et al. [54] observed 42.4 % loss of bioactive compounds in nanoemulsion during storage for 8 weeks at 20 ^{o}C.

4.3.17.2. Effect on emulsion stability

The emulsion stability index (ESI) indicated that nanoemulsion produced under optimized conditions was stable and resistant to gravitational phase separation. During

storage at 25 ℃, emulsion colour faded rapidly as compared to 6 ℃, indicating greater extent of carotenoids degradation, despite showing physical stability **(Fig 4.16).**

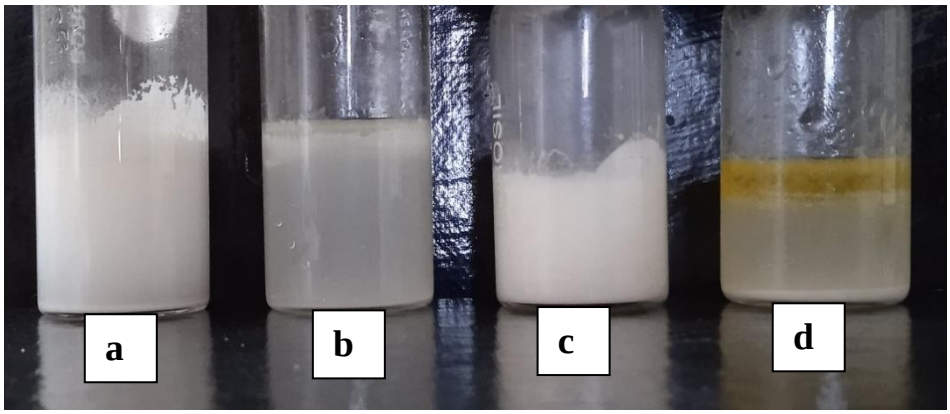

Fig. 4.16. Storage stability of emulsion after 35 days: (a) Storage at 25 ℃ with HPH treatment, (b) Storage at 25 ℃ without HPH treatment, (c) Storage at 6 ℃ with HPH treatment, and (d) Storage at 6 ℃ without HPH treatment.

The high surface area of nanoemulsion may have promoted carotenoids degradation and loss [57]. As shown in **Fig. 4.17,** the ESI reduction rate of carotenoids in C-HP-US-StNE at 25 ℃ was 3-fold (3.43) higher than that stored at 6 ℃. Emulsion storage at higher temperature exhibited the highest rate of gravitational separation/creaming.

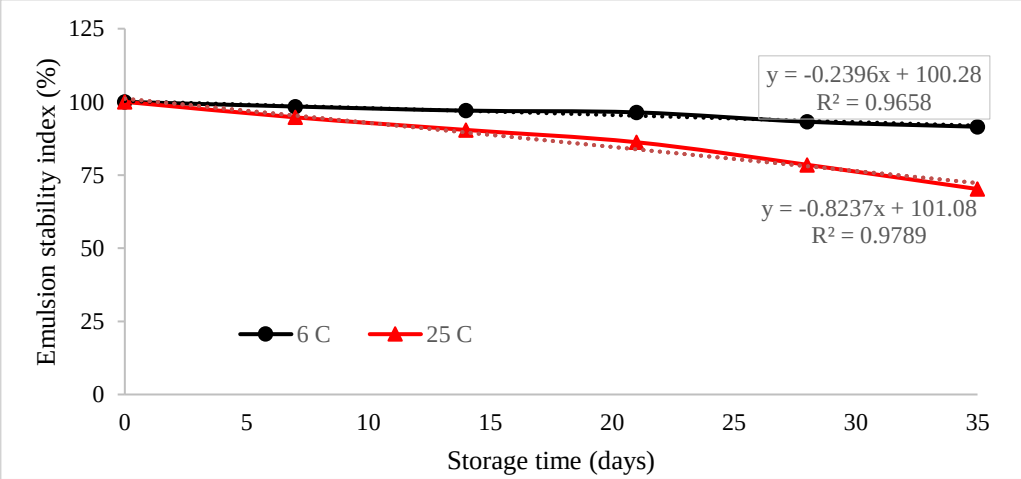

Fig. 4.17. Stability of nanoemulsions stored at 6 and 25 ℃.

Olive oil concentration of 3-5% was reported to show maximum emulsion stability [51]. Olive oil hampers Ostwald ripening by gaining the entropy from oil mixing [51] as a result higher stability was observed. Li et al. [34] reported no creaming of starch-stabilized nanoemulsion up to 2 months storage.

4.4. Conclusion

Ultrasonication and subsequent HPH treatment readily fragmented corn starch to nanosize in an aqueous solution and the physical treatments and carotenoids enrichment of starch nanoparticle enhanced the thermal stability of the starch powder. DSC and TGA treatments for closed and open systems respectively were found to be efficient to study the thermal properties of physically modified starches. These starch nanoparticles were able to stabilize Pickering emulsion of olive oil enriched with carotenoids extracted from passion fruit peel. The nanoemulsion was stable when subjected to heat and freeze-thaw treatments. It is suggested that combination of physical treatments of starch particles could be applied in the food processing industry to develop natural and chemical-free nanosized emulsifying agents. The starch nanoparticles enriched with bioactive compounds (carotenoids) extracted from fruit waste as source material will enhance the waste management and the powder can be applied as a functional ingredient in new food product development.

Bibliography

[1] Adeyeye, E., Ekiti, A. and Aremu, M. O. Chemical Composition of the Raw Fruit Coat, Seed and Pulp of Passion Fruit (*Passiflora edulis*). *FUW Trends in Science & Technology Journal*, 2(1):334–341, 2017.

[2] Apostolidis, E. and Mandala, I. Modification of resistant starch nanoparticles using high-pressure homogenization treatment. *Food Hydrocolloids*, 103:105677, 2020.

[3] Asua, J. M. Miniemulsion polymerization. *Progress in Polymer Science*, 27(7):1283–1346, 2002.

[4] Boufi, S. et al. Ultrasonic assisted production of starch nanoparticles : Structural characterization and mechanism of disintegration. *Ultrasonics Sonochemistry*, 41:327–336, 2018.

[5] Buckow, R., Heinz, V. and Knorr, D. High pressure phase transition kinetics of maize starch. *Journal of Food Engineering*, 81(2):469–475, 2007.

[6] Caicedo Chacon, W. D., Ayala Valencia, G., Aparicio Rojas, G. M. and Agudelo Henao, A. C. Mathematical Models for Prediction of Water Evaporation and Thermal Degradation Kinetics of Potato Starch Nanoparticles Obtained by Nanoprecipitation. *Starch/Staerke*, 71(1–2): 2019.

[7] Calligaris, S. et al. Nanoemulsion preparation by combining high pressure homogenization and high power ultrasound at low energy densities. *Food Research*

International, 8:25–30, 2016.

[8] Carvalho, L. M. J. et al. Total carotenoid content, α-carotene and β-carotene, of landrace pumpkins (*Cucurbita moschata Duch*): A preliminary study. *Food Research International*, 47(2):337–340, 2012.

[9] Choi, H. D. et al. Starch nanoparticles produced via acidic dry heat treatment as a stabilizer for a Pickering emulsion: Influence of the physical properties of particles. *Carbohydrate Polymers*, 239 116241, 2020.

[10] Chutia, H., Mahanta, C. L., Ojah, N. and Choudhury, A. J. Fuzzy logic approach for optimization of blended beverage of cold plasma treated TCW and orange juice. *Journal of Food Measurement and Characterization*, 14 (4):1926–1938, 2020.

[11] Cinelli, G. et al. Red wine-enriched olive oil emulsions: Role of wine polyphenols in the oxidative stability. *Colloids and Interfaces*, 3(3): 2019.

[12] Corrêa, R. C. G. et al. The past decade findings related with nutritional composition, bioactive molecules and biotechnological applications of *Passiflora spp*. (passion fruit). *Trends in Food Science and Technology*, 58:79–95, 2016.

[13] Cruz-Orea, A., Pitsi, G., Jamée, P. and Thoen, J. Phase transitions in the starch-water system studied by adiabatic scanning calorimetry. *Journal of Agricultural and Food Chemistry*, 50(6):1335–1344, 2002.

[14] Dammak, I., Sobral, P. J. do A., Aquino, A., Neves, M. A. das and Conte-Junior, C. A. Nanoemulsions: Using emulsifiers from natural sources replacing synthetic ones—A review. *Comprehensive Reviews in Food Science and Food Safety*, 19(5):2721–2746, 2020.

[15] Ding, Y. and Kan, J. Optimization and characterization of high pressure homogenization produced chemically modified starch nanoparticles. *Journal of Food Science and Technology*, 54(13):4501–4509, 2017.

[16] Elik, A., Yanik, D. K. and Göğüş, F. Microwave-assisted extraction of carotenoids from carrot juice processing waste using flaxseed oil as a solvent. *LWT - Food Science and Technology*, 123:109100, 2020.

[17] Evans, I. D. and Haisman, D. R. The Effect of Solutes on the Gelatinization Temperature Range of Potato Starch. *Starch - Stärke*, 34(7):224–231, 1982.

[18] Fellows, P. J. *Food Processing Technology: Principles and Practice*. *Food Processing Technology: Principles and Practice*, 2013.

[19] Guo, Z., Zhao, B., Chen, L. and Zheng, B. Physicochemical Properties and Digestion of Lotus Seed Starch under High-Pressure Homogenization. *Nutrients*,

11:371, 2019.

[20] Gurpreet, K. and Singh, S. K. Review of nanoemulsion formulation and characterization techniques. *Indian Journal of Pharmaceutical Sciences*, 80(5):781–789, 2018.

[21] Haaj, S. B., Magnin, A. and Boufi, S. Starch nanoparticles produced via ultrasonication as a sustainable stabilizer in Pickering emulsion polymerization. *RSC Advances*, 4(80):42638–42646, 2014.

[22] He, L., Li, X., Li, W., Yuan, J. and Zhou, H. A method for determining reactive hydroxyl groups in natural fibers: Application to ramie fiber and its modification. *Carbohydrate Research*, 348:95–98, 2012.

[23] Hsu, B. Y., Pu, Y. S., Inbaraj, B. S. and Chen, B. H. An improved high performance liquid chromatography-diode array detection-mass spectrometry method for determination of carotenoids and their precursors phytoene and phytofluene in human serum. *Journal of Chromatography B*, 899:36–45, 2012.

[24] Jia, J. et al. Effect of ultrasound treatment on physicochemical and functional properties of wheat germ globulin. *Nongye Jixie Xuebao/Transactions of the Chinese Society of Agricultural Machinery*, 40(8):105–110, 2009.

[25] Jimenez-Escobar, M. P. et al. In vitro and In vivo antioxidant properties of paprika carotenoids nanoemulsions. *LWT - Food Science and Technology*, 118:108694, 2020.

[26] Karacam, C. H., Sahin, S. and Oztop, M. H. Effect of high pressure homogenization (microfluidization) on the quality of Ottoman Strawberry (*F. Ananassa*) juice. *LWT-Food Science and Technolog*, 64(2):932–937, 2015.

[27] Karimi, N. and Mohammadifar, M. A. Role of water soluble and water swellable fractions of gum tragacanth on stability and characteristic of model oil in water emulsion. *Food Hydrocolloids*, 37:124–133, 2014.

[28] Kaur, H. and Gill, B. S. Effect of high-intensity ultrasound treatment on nutritional, rheological and structural properties of starches obtained from different cereals. *International Journal of Biological Macromolecules*, 126:367–375, 2019.

[29] Kim, H. Y., Park, D. J., Kim, J. Y. and Lim, S. T. Preparation of crystalline starch nanoparticles using cold acid hydrolysis and ultrasonication. *Carbohydrate Polymers*, 98(1):295–301, 2013.

[30] Krishnakumar, T. and Sajeev, M. S. Effect of Ultrasound Treatment on Physicochemical and Functional Properties of Cassava Starch. *International*

Journal of Current Microbiology and Applied Sciences, 7(10):3122–3135, 2018.

[31] Lante, A. and Friso, D. Oxidative stability and rheological properties of nanoemulsions with ultrasonic extracted green tea infusion. *Food Research International*, 54(1):269–276, 2013.

[32] Lante, A., Nardi, T., Zocca, F., Giacomini, A. and Corich, V. Evaluation of red chicory extract as a natural antioxidant by pure lipid oxidation and yeast oxidative stress response as model systems. *Journal of Agricultural and Food Chemistry*, 59(10):5318–5324, 2011.

[33] Lecorre, D., Bras, J. and Dufresne, A. Influence of native starch ' s properties on starch nanocrystals thermal properties. *Carbohydrate Polymers* , 87:658–666, 2012.

[34] Li, C., Sun, P. and Yang, C. Emulsion stabilized by starch nanocrystals. *Starch/Starke*, 64:497–502, 2012.

[35] Li, G. and Zhu, F. Effect of high pressure on rheological and thermal properties of quinoa and maize starches. *Food Chemistry*, 241:380–386, 2018.

[36] Li, H. et al. Insights into maize starch degradation by high pressure homogenization treatment from molecular structure aspect. *International Journal of Biological Macromolecules*, 161:72–77, 2020.

[37] Liu, D., Wu, Q., Chen, H. and Chang, P. R. Transitional properties of starch colloid with particle size reduction from micro to nanometer. *Journal of Colloid And Interface Science*, 339:117–124, 2009.

[38] Liu, X. et al. Thermal degradation and stability of starch under different processing conditions. *Starch/Sta¨rke*, 65:48–60, 2013.

[39] Liu, Y. et al. Effect of ultra-high pressure homogenization on microorganism and quality of composite pear juice. *Food Science & Nutrition*, 10:3072–3084, 2022.

[40] Liu, Y., Yang, L., Ma, C. and Zhang, Y. Thermal behavior of sweet potato starch by non-isothermal thermogravimetric analysis. *Materials*, 12(5):699, 2019.

[41] Lozano-Navarro, J. I. et al. Chitosan-starch films with natural extracts: Physical, chemical, morphological and thermal properties. *Materials*, 11(1):1–20, 2018.

[42] Mahbubul, I. M. Stability and Dispersion Characterization of Nanofluid. *Preparation, Characterization, Properties and Application of Nanofluid*, 47–112, 2019.

[43] Maoka, T. Carotenoids as natural functional pigments. *Journal of Natural Medicines*, 74(1): 2020.

[44] Martins, A. et al. Ultrasonic modification of purple taro starch (Colocasia esculenta

B . Tini): structural , psychochemical and thermal properties. *Journal of Thermal Analysis and Calorimetry*, 142(2):819–828, 2020.

[45] Merci, A., Mali, S. and Carvalho, G. M. de. Waxy maize, corn and cassava starch: Thermal degradation kinetics. *Semina: Ciências Exatas e Tecnológicas*, 40(1):13, 2019.

[46] Naseema, A., Kovooru, L., Behera, A. K., Kumar, K. P. P. and Srivastava, P. A critical review of synthesis procedures, applications and future potential of nanoemulsions. *Advances in Colloid and Interface Science*, 102318, 2020.

[47] Park, E. Y., Kim, M. J., Cho, M., Lee, J. H. and Kim, J. Y. Production of starch nanoparticles using normal maize starch via heat-moisture treatment under mildly acidic conditions and homogenization. *Carbohydrate Polymers*, 151:274–282, 2016.

[48] Perez Herrera, M., Vasanthan, T. and Chen, L. Rheology of starch nanoparticles as influenced by particle size, concentration and temperature. *Food Hydrocolloids*, 66:237–245, 2017.

[49] Pigłowska, M., Kurc, B., Rymaniak, Ł., Lijewski, P. and Fu´, P. Kinetics and Thermodynamics of Thermal Degradation of Di ff erent Starches and Estimation the OH Group and H2O Content on the Surface by TG/DTG-DTA. *Polymers*, 12(2):357, 2020.

[50] dos Reis, L. C. R., Facco, E. M. P., Salvador, M., Flôres, S. H. and Rios, A. de O. Antioxidant potential and physicochemical characterization of yellow, purple and orange passion fruit. *Journal of Food Science and Technology*, 55(7):2679–2691, 2018.

[51] Ren, J. N., Dong, M., Hou, Y. Y., Fan, G. and Pan, S. Y. Effect of olive oil on the preparation of nanoemulsions and its effect on aroma release. *Journal of Food Science and Technology*, 55(10):4223–4231, 2018.

[52] Romanski, F. S., Jayjock, E., Muzzio, F. J. and Tomassone, M. S. Important Factors in the Size Reduction of Polymer-Stabilized Drug Particle Suspensions Using High-Pressure Homogenization. *J Pharm Innov*, 6:97–106, 2011.

[53] Rueda-Ordóñez, Y. J. and Tannous, K. Drying and thermal decomposition kinetics of sugarcane straw by nonisothermal thermogravimetric analysis. *Bioresource Technology*, 264:131–139, 2018.

[54] Ruiz-Montañez, G., Ragazzo-Sanchez, J. A., Picart-Palmade, L., Calderón-Santoyo, M. and Chevalier-Lucia, D. Optimization of nanoemulsions processed by

high-pressure homogenization to protect a bioactive extract of jackfruit (Artocarpus heterophyllus Lam). *Innovative Food Science and Emerging Technologies*, 40:35–41, 2016.

[55] Sandhu, K. S. and Nain, V. Plant Biotechnology: Recent Advancements and Developments. *Starch nanoparticles: Their preparation and applications*, 213–232, 2017.

[56] Sicaire, A. G. et al. Ultrasound induced green solvent extraction of oil from oleaginous seeds. *Ultrasonics Sonochemistry*, 31:319–329, 2016.

[57] Sotomayor-Gerding, D. et al. High carotenoid bioaccessibility through linseed oil nanoemulsions with enhanced physical and oxidative stability. *Food Chemistry*, 199:463–470, 2016.

[58] Spychaj, T., Wilpiszewska, K. and Zdanowicz, M. Medium and high substituted carboxymethyl starch: synthesis, characterization and application. *Starch/Staerke*, 65(2):22–33, 2006.

[59] Wang, B. et al. Effect of high-pressure homogenization on the structure and thermal properties of maize starch. *Journal of Food Engineering*, 87(3):436–444, 2008.

[60] Wei, B., Cai, C., Jin, Z. and Tian, Y. High-pressure homogenization induced degradation of amylopectin in a gelatinized state. *Starch/Stärke*, 68:734–741, 2016.

[61] Xinde, X., Shanjing, Y., Ning, H. and Bin, S. Measurement and influence factors of the flowability of microcapsules with high-content β-carotene. *Chinese Journal of Chemical Engineering*, 15(4):579–585, 2007.